ISSN: 2588-5596

JGT

Journal of Gas Technology

Volume 8 . Issue 1 . Summer 2023 . www.jgt.irangi.org

Journal of Gas Technology, JGT

Volume 8, Issue 1, Summer 2023

Publisher
Iranian Gas Institute

Contact Information
http://jgt.irangi.org
Email: ijgt.igi@gmail.com

EISSN: 2588-5596

Open Access Journal
Journal of Gas Technology is a peer reviewed, open access journal.

JOURNAL OF GAS TECHNOLOGY

Volume 8, Issue 1, Summer 2023

Annual Names of Reviewers

Ali Vatani
University of Tehran

Mastaneh Hajipour
Islamic Azad University, Science and Research Branch

Rahbar Rahimi
University of Sistan and Baluchestan

Saeid Jamshidi
Sharif University of Technology

Amir Hossein Mohammadi
University of KwaZulu-Natal, South Africa

Masoud Aghajani
Petroleum University of Technology

Morteza Zivdar
University of Sistan and Baluchestan

Reza Mohebian
University of Tehran

Mahdi Moayed Mohseni
Islamic Azad University, Science and Research Branch

Sepideh Amiri Tavasoli
Hormozgan Province Gas Company

kamran keynejad
University of Tehran

Seyed Mohsen Peyghambarzadeh
Islamic Azad University, Mahshahr branch

Yahya Balouchi
University of Sistan and Baluchestan

Leila Moharrery
Islamic Azad University, Robat Karim Branch

Farnaz Karbasi
Islamic Azad University, South Tehran Branch

Ebrahim Biniaz Delijani
Islamic Azad University, Science and Research Branch

Table of Contents

Numerical Simulation in a Dynamic Regime of Natural Gas Flow in the Pipeline Networ 5

Rabah Haoui

Probing Methane Adsorption in MIL Metal-Organic Frameworks using Molecular Dynamics Simulations 15

Saman Banijamali, Hedayat Azizpour, Parissa Khadiv-parsi

A Novel Method for Heat Integration of Natural Gas Sweetening Process 25

Ehsan Fatehi, Parisa Sadat Fatemi, Mohammad Javad Zarkesh, Mahshid Moradi, Shahab Taleghani, Mahsa Majidi

Synthesis and Characterization of Glycidyl Methacrylate-Grafted Ethylene-Propylene Diene Terpolymer Employing Styrene as a Comonomer 35

Marzieh Alidadi-Shamsabadi, Shirin Shokoohi

JOURNAL OF GAS TECHNOLOGY

Volume 8 /Issue 1 / Summer 2023 / Pages 5-14

Journal Home page: http://jgt.irangi.org

Numerical Simulation in a Dynamic Regime of Natural Gas Flow in the Pipeline Network

Rabah Haoui*

University Of Sciences and Technology Houari Boumediene, Department of Thermal Energetics, Algiers, Algeria

ARTICLE INFO

ORIGINAL RESEARCH ARTICLE

Article History:
Received: 28 June 2023
Revised: 25 July 2023
Accepted: 20 August 2023

Keywords:
Natural gas consummation
Network of natural gas
Unsteady flow
Compressible flow
Dynamic regime
Finite difference method

ABSTRACT

The purpose of this article is to present a comment manifests the pressure and flow supply in the case of consumptions in dynamic regime. The mathematical model is a system of nonlinear differential equations dealing with a compressible flow with the term of pressure drops, the temperature is considered constant and equal to that of the environment. The boundary conditions are given and the initial solution is unspecified, after the transitory solution, the periodic dynamic mode is established in a stable way. The discretization method used is that of fine differences with a structured mesh. The method of resolution is semi-implicit with a step of time which strongly depends on the number of CFL which ensures convergence. The chosen method is stable over time. The main results obtained are the validity of the method used to solve a dynamic problem, the precision of the calculations and the physical phenomenon which is clearly visible from the distribution of pressures and flow rates as a function of time and position.

DOR: 20.1001.1/JGT.2024.2015754.1031

How to cite this article
R. Haoui, Numerical Simulation in a Dynamic Regime of Natural Gas Flow in the Pipeline Network. Journal of Gas Technology. 2023; 8(1): 5-14.
(http://jgt.irangi.org/article_712119.html)

* Corresponding author.
E-mail address: haoui_rabah@yahoo.fr, (R. Haoui).

Available online 20 September 2023

1. Introduction

The study of the flow of natural gas in pipeline networks is of great importance in the distribution according to the needs of industrial consumers. If the consumption does not vary over time, the flow regime is purely stationary and the system of equations can be solved explicitly by an iterative method. On the other hand, in the case where the customers' consumption varies as a function of time over a period of 24 hours, the regime is then dynamic and the system contains non-linear unsteady differential equations. The method used in solving the problem is the finite difference method taking into account a given initial solution and the boundary conditions at the level of each consumption point. Of course that at the beginning of calculation the solution is purely in transient mode, after a few hours one reaches the periodic mode at the entry of supply pipe. Each section of the pipes is divided into several meshes in such a way that the friction coefficient and the compressibility factor can be considered constant. The time step is calculated to ensure the convergence of the calculation code with a CFL=0.4 for one supply pipe and 0.005 for two supplies pipes in the dynamic case, the results do not change for a CFL lower than 0.005. In the work of Farzaneh (2006), the unsteady resolution was not done using finite elements but by an integration where the variables p and t were taken as independent. The same in the work of Pambour (2015), where he used a numerical approach and the speed of the flow was neglected in front of the speed of sound, these results were compared to those of Simone. On the other hand, WangHai (2011) used the finite volume method with a semi-implicit scheme but the comparison was not made between the input and the output at the same time. Shanbi (2013) used the Newton-Raphson method as a technical solution between the different nodes of the network but he did not give information on the unsteady state in the pipes between the nodes.

2. Master Equations

The conservative equations governing the one-dimensional compressible flow are the equation of continuity, momentum and state since the flow is assumed isothermal at the ambient temperature, equations system used also by Farzaneh (2016).

$$\frac{\partial \rho}{\partial t} + \frac{\partial (\rho V)}{\partial x} = 0 \tag{1}$$

$$\frac{\partial (\rho V)}{\partial t} + \frac{\partial (\rho V^2 + p)}{\partial x} + \frac{\lambda}{2d} \rho V |V| = 0 \tag{2}$$

$$\frac{p}{\rho} = zrT \tag{3}$$

The compressibility factor is given by $z = f(p_r et\ T_r)$

Where ρ, V and p are the density, velocity and pressure of flow respectively. Equations (1) and (2) constitute the nonlinear partial differential equation system to be solved.

Berthelot established a more general relation for the determination of the compressibility factor:

$$z(p,T) = 1 + \frac{9}{128} \frac{p}{p_c} \frac{T_c}{T} \left(1 - \frac{6T_c^2}{T^2}\right) \tag{4}$$

At constant temperature the compressibility factor takes the form:

$$Z(p,T) = 1 - a.p \ \ (a > 0) \tag{5}$$

Where p_r and T_r are the reduced pressure and temperature such that:

$$p_r = \frac{p}{p_c} \ \ ; \ \ T_r = \frac{T}{T_c} \tag{6}$$

The average pseudo-critical pressure and pseudo-critical temperature of the gas mixture for a given mole fractions x_i of gas components are given by:

$$p_{cm} = \sum x_i p_{ci} \quad ; \quad T_{cm} = \sum x_i T_{ci} \tag{7}$$

In the following (Table.1) some gases are given with the critical temperature and pressure, Pascal (1972).

Table 1. Critical Pressure and Temperature for Natural Gas

Gas	Molecular weight (g/mol)	Boiling T (°C) at 1 bar	p_c (bars)	T_c (°C)
Methane CH_4	16.04	-161.58	45.80	-82.10
Ethane C_2H_6	30.07	-88.63	48.20	32.27
Propane C_3H_8	44.09	-42.06	42.00	96.81
Butane C_4H_{10}	58.12	-0.5	35.47	152.0
Isobutane	58.12	-11.72	36.40	134.9
Pentane C_5H_{12}	72.15	+27.85	32.90	197.2
Azote N_2	28.02	-195.78	33.49	-13.147

If we have the density d_{NG} of natural gas directly, the law used is that of the $CNGA$ (California Natural Gas Association):

$$\frac{1}{Z} = 1 + \left(344400\ 10^{(1.785 d_{NG})} \frac{p}{T^{3.825}}\right);\ p(psia), \qquad T(°R) \tag{8}$$

This method is used for pressures gauge p above 7 bar. For pressures below 7 bars, the compressibility factor is taken as unity.

The density of natural gas varies according to the composition, generally it is around 0.6. It can be determined by the relationship:

$$d_{NG} = \frac{M_{GN}}{M_{air}} \tag{9}$$

With

$$M_{NG} = \sum X_s M_s \tag{10}$$

Where M_{NG} is the molar mass of the mixture, M_s and X_s are the molar mass and molar fraction of species s respectively.

An expression for the head loss coefficient λ valid for turbulent flow in pipeline transportation used in the article Hofer (1973), called Hofer's formula.

$$\lambda = \left\{2 \log_{10}\left[\frac{4.518}{Re} \log_{10}\left(\frac{Re}{7}\right)^{1.11} + \frac{e/d}{3.71}\right]\right\}^{-2} \tag{11}$$

Cited in paper of K. A. Pambour et all (2015). Ther are many expressions of loss coeffition in litterature, see Ouyang (1996). Re is the reynolds number, e the absolute pipe roughness and d the pipe diameter.

3. Resolution Method

Since the flow is one-dimensional with nonlinear differential equations, the finite difference method is largely sufficient to solve the problem. Partial derivatives are replaced by finite differences. The temporal term is solved by a semi-explicit method, for example:

$$\frac{\partial F(i)}{\partial x} = \frac{F(i+1) - F(i-1)}{2\Delta x} \tag{12}$$

$$\frac{\partial F(i)}{\partial t} = \frac{F(i)^{n+1} - F(i)^n}{\Delta t} \tag{13}$$

The numerical resolution of the system of equation requires an initial solution and boundary conditions. If the initial solution is not real, the periodic dynamic regime is obtained after a transient regime after a few hours or a few ten hours if the pipe-line is longer. Convergence is ensured with a time step such as, Klaus (1996):

$$\Delta t = min\left[\left(\frac{\Delta x.\, CFL}{|V(i)| + a(i)}\right), \left(\frac{(\Delta x)^2.\, CFL}{2\,\mu/\rho\,(i)}\right)\right] \tag{14}$$

Where a is the speed of sound.

Concerning the boundary conditions, at the inlet the pressures are given and a single variable is extrapolated, at the outlet, the flow rates are known and two quantities are extrapolated, the others are therefore calculated. At the

junction point J as represented in (Figure 1), the conservation of mass equation is used in its integral form to determine the instantaneous density at this point and therefore the pressure by using the equation of state, Pambour (2015).

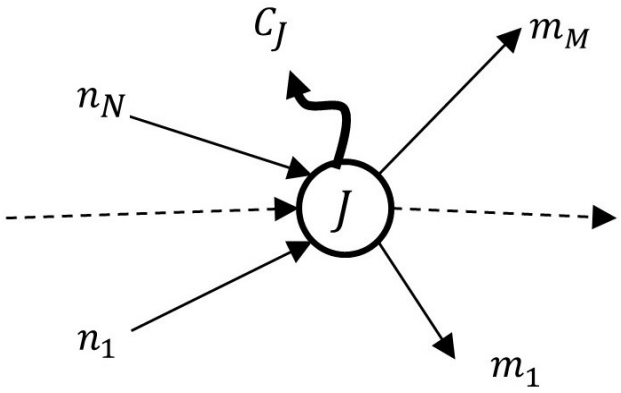

Figure 1. Presentation of Junction in Network

We have:

$$\int_v \frac{\partial \rho}{\partial t}.dv + \int_s \rho.(\vec{V}.\vec{n})\,ds = 0 \;\; ; \;\; [k\,g/s] \qquad (15)$$

This give:

$$\frac{\rho(i)^{n+1} - \rho(i)^n}{\Delta t}.volume + \sum_{m=1}^{M} \rho_{Jm}.V_{Jm}.S_m - \sum_{n=1}^{N} \rho_{Jn}.V_{Jn}.S_n = C_J \qquad (16)$$

Where C_J is the consumption at the junction point if exist.

The control volume is such as:

$$volume = \sum_{n=1}^{N} (S.\Delta x)_n + \sum_{m=1}^{M} (S.\Delta x)_m \qquad (17)$$

The pressure is calculated from the equation of state:

$$p_J = z.r.T.\rho_J \qquad (18)$$

4. Application and Comparison

In dynamic mode, the consumptions are not generally constant; they are variable at the nodes where the customers are. Consumption at each network outlet is given as a function of time (Q,t). The flow in the gas pipeline is therefore in an unsteady state. The variation of the flow rate or the pressure at the outlet of a pipe influences all the parameters throughout the pipe (Figure 2).

The pressure at supply point A is assumed to be constant $p(A,t) = p_A$, the consumption at points C_1 and C_2 are variable, the boundary conditions are $Q_1(C_1,t) = f(t)$ and $Q_2\ (C_2,t) = f(t)$ or else $P_1\ (C_1,t) = f(t)$ and $P_2\ (C_2,t) = f(t)$. The initial solution is preferably unknown if the network is already in operation. To do this, either we take the initial solution of a permanent flow or it starts from the state at rest. In this case, two flow regimes arise, the first is transient and the second is the periodic regime.

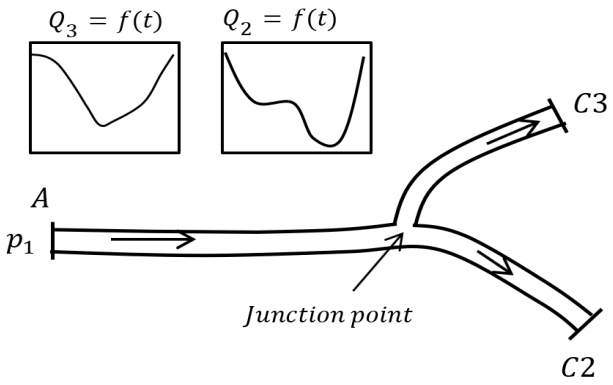

Figure 2. Typical Network for two Consumptions

4.1. Static Simulation

The supply pressure gauge at point A is 50bar and at consumption points C_1 and C_2 the pressure gauge is 5bar. Let us test the unsteady state computation with the finite difference method using an explicit first-order scheme. The length and the diameter of the three pipes are the same, the density of the natural gas is taken equal to 0.6 which gives a constant of gas r = 478.47 J/kg.K. Convergence is obtained after a certain number of iterations when the residual is less than 10^{-6} where the quantities stabilize and steady flow is obtained (Figure 3).

The time here is an iterative parameter. The calculation converges towards the stationary solution with the flow rate q_{m2} = 214 kg/s, different from the analytical solution q_{m2} = 213 kg/s given by the equation of a stationary flow such as:

$$q_m^2 = \frac{\pi^2 d^4}{16rzT} \frac{p_{inl}^2 - p_{out}^2}{\lambda \frac{L}{d} + 2\,ln\left(\frac{p_{inl}}{p_{out}}\right)} \qquad (19)$$

The 0.4% difference is caused by the accuracy of the calculations. If we increase the number of nodes, the computation time becomes enormous. The computer code is stable. The convergence took place at a residue on the density of the order 10^{-6}.

$$q_{m2} = 214.13 \text{ kg/s} \quad ; q_{m3} = 214.13 \text{ kg/s}$$

$$q_{m1} = 428.45 \text{ kg/s}$$

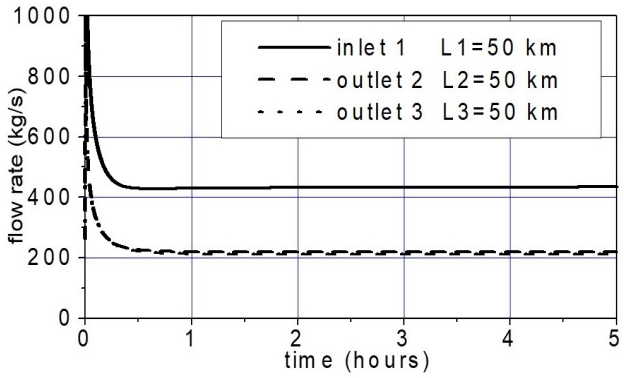

Figure 3. Flow Rate Versus Time

The variation of the density at the junction point during the iterations is given by the following graph (Figure 4):

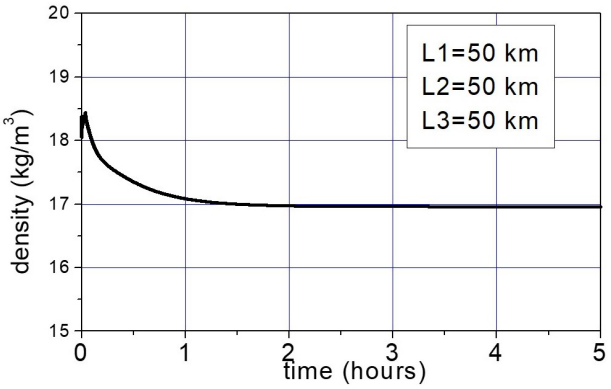

Figure 4. Density Variation in Junction Point Versus Time

Let's increase the length of pipe ② to100 km (Figure 5) ; the flow rate becomes less than that of pipe ③.

$$q_{m2} = 171.63 \text{ kg/s} \quad ; q_{m3} = 241.65 \text{ kg/s}$$

$$q_{m1} = 413.62 \text{ kg/s}$$

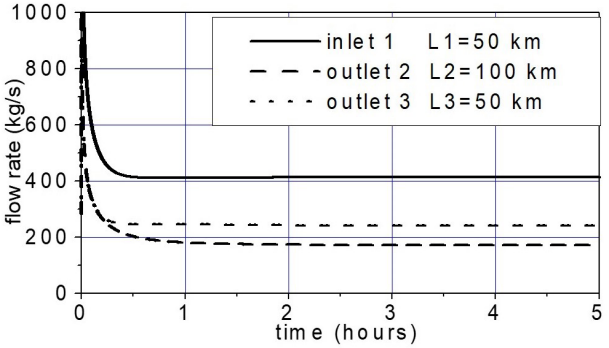

Figure 5. Flow Rate Versus Time

4.2. Reserve of Gas (One Pipe)

This unsteady state can also be used to determine the emptying time or the gasometrical reserve. As soon as steady state is reached after 0.6 hours, it is allowed to operate until t=2 hours. A gas cut is made at the inlet of the pipe and the outlet pressure is always maintained at 5 bars, an emptying time of 1h8min is obtained. The calculation is stopped when the pressure at the pipe inlet becomes equal to the outlet pressure. The calculation gives a gas reserve:

```
reserve in kg =  835574.654531091900000
reserve in MMSCM =       1.136966004064116
reserve in hours =       1.111510051879290
Stop - Program terminated.
```

Note that in this case the output is directly connected to a consumer operating with a set point pressure equal to 5 bars. This means that consumption drops after the gas breaks (Figure 6 to 8). The 1 h 8 min emptying time is much higher compared to the case where the consumption was supposed to be invariable q_m = 479.37 kg/s calculated analytically and t = 28 min. In the case where only the pressure is imposed at the outlet, the consumption is calculated numerically using the finite difference method, the usable gas reserve in mass is the difference between the mass contained in the pipe at the time of the cut and the remaining mass when the pressure is everywhere equal to p_s = 5 bars, i.e. :

$$M(kg) = \sum_{1}^{i_m-1} \frac{(\rho_i + \rho_{i+1})}{2}.S.dx - \frac{p_s}{rT}.S.L \qquad (20)$$

Or in standard m³ such as:

$$V = \frac{M(kg)}{\rho} = \frac{M(kg)}{p_a}.r.T_a \qquad (21)$$

With: p_a = 1 atm et T_a = 15 °C.

It must be the same; it is the consumption time of the reserve that is deferring. The (Figure 9) shows the effect of the mesh refinement on the gasometrical reserve, the error is only 0.5% when going from 50 meshes to 1000 meshes. We observe the consistency of the calculation code when the step $\Delta x \rightarrow 0$.

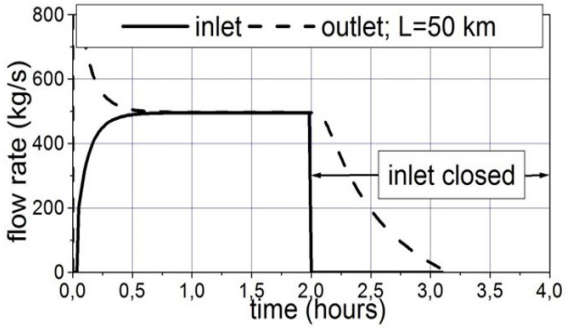

Figure 6. Flow Rate Versus Time and Reserve

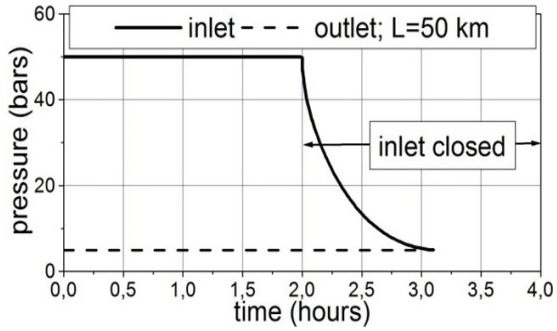

Figure 7. Pressure Versus Time and Reserve

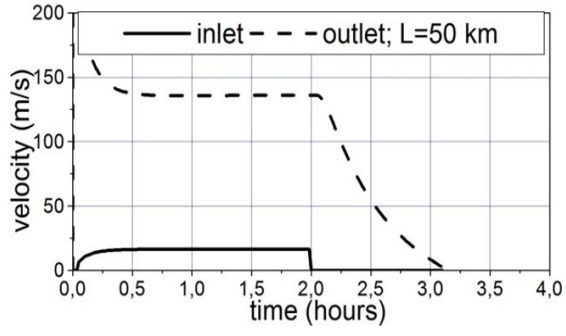

Figure 8. Velocity Versus Time

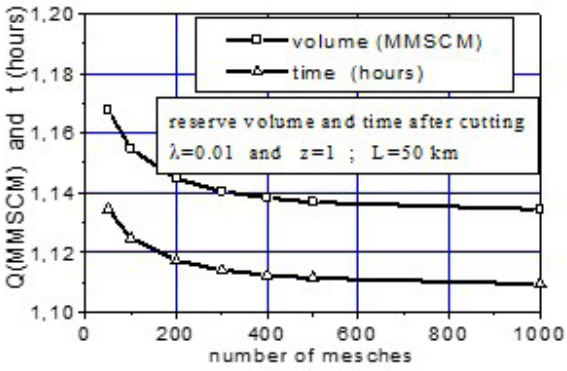

Figure 9. Effect of the Mesh Refinement on the Reserve

4.3. Dynamic Simulation

4.3.1. Case of Two Consumptions and one Supply

We test a real case of two consumptions given in the following tables (Figure10):

$$L1 = 600\ km \quad \emptyset 1 = 389\ mm$$

Table 2. Pipeline Consumption at Outlet 2

$L2 = 5km$; $\emptyset 2 = 310mm$			
t (heures)	Q_2 (m³ S/h)	t (heures)	Q_2 (m³ S/h)
0:00	8000	12:00	30000
1:00	10000	13:00	50000
2:00	11000	14:00	50000
3:00	13000	15:00	70000
4:00	14000	16:00	80000
5:00	16000	17:00	70000
6:00	20000	18:00	70000
7:00	25000	19:00	65000
8:00	25000	20:00	50000
9:00	26000	21:00	40000
10:00	27000	22:00	30000
11:00	28000	23:00	20000

Table 3. Pipeline Consumption at Outlet 3

$L3 = 3km \ ; \ \emptyset 3 = 206mm$			
t (heures)	Q_2 (m^3 S/h)	t (heures)	Q_2 (m^3 S/h)
0:00	2000	12:00	15000
1:00	2500	13:00	20000
2:00	3000	14:00	12000
3:00	3000	15:00	15000
4:00	3700	16:00	18000
5:00	4000	17:00	19000
6:00	5000	18:00	22000
7:00	5200	19:00	21000
8:00	6000	20:00	19000
9:00	6500	21:00	17000
10:00	9000	22:00	15000
11:00	10000	23:00	11000

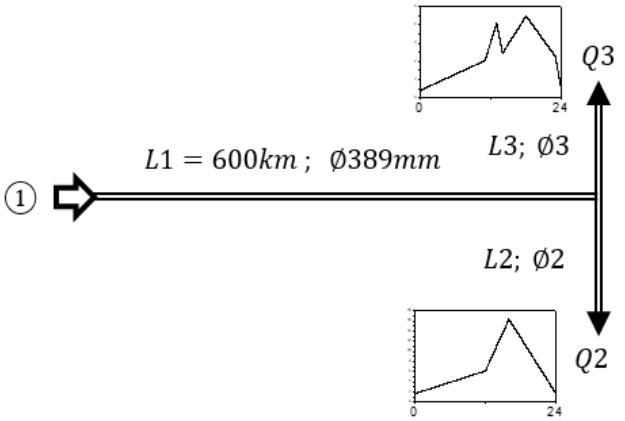

Figure 10. Two Consumptions and One Supply

The density of natural gas is 0.6. The real initial solution does not exist as a preliminary; the periodic solution is obtained after 48h preceded by the transient solution (Figure 11) . The objective is to determine the variation of the pressure as function of time at the outlet of the consumption pipes ② and ③ as well as the variation of the flow at the inlet of the supply pipe ①. It should be remembered that the pressure drop coefficient has a considerable influence on the results. The flow rate at the inlet is also function of time (Figure 12).

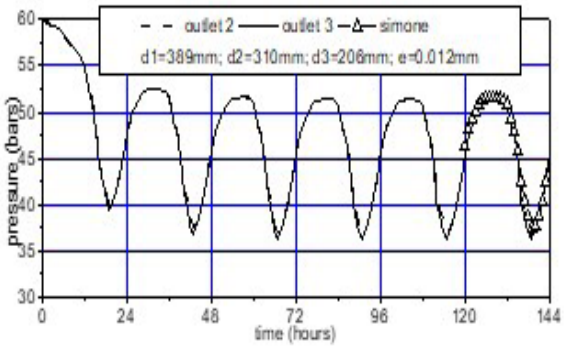

Figure 11. Periodic Pressure at Outlet

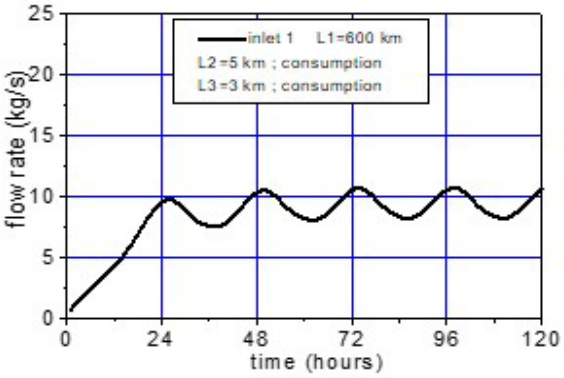

Figure 12. Flow Rate at Inlet Versus Time

In a time interval equal to the period, the mass of gas entering the network equals the mass consumed. By numerical integration we find (Figure 13):

$$Q_1 = 954240 \ kg \quad ; \quad Q_2 = 727799 \ kg$$

$$Q_3 = 226572 \ kg$$

This confirms the precision of the convergence and the consistency of the calculation code.

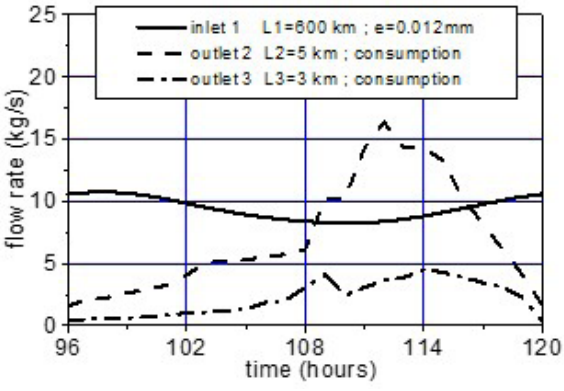

Figure 13. Flow rate of Periodic Regime versus Time

Now we are going to suppose consumption at the junction point J where $C_{jonction}$=20000 m^3 S/h in a continuous way (Figure 14). In this case the rate flow at inlet of pipe increases and consequently the losses in the network, this requires lower pressures at the outlet of each pipe. The mass entering the pipe for $C_{jonction}$ = 20000 m^3 S/h is found to be equal to 1286560 kg instead of 954240 kg. The periodic regime is obtained after 72 hours. The following graphs show the variation of the flow at the inlet of the pipe (Figure 15) and the pressures at the points of consumption (Figure 16) . The solution is stable if the code is left running for longer. The (Figure 17) shown the variation of flow rate at the inlet and outlets in periodic regime.

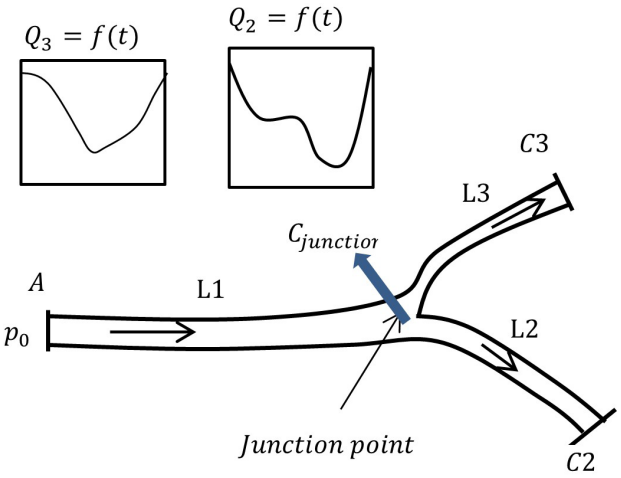

Figure 14. Network with Junction Consumption

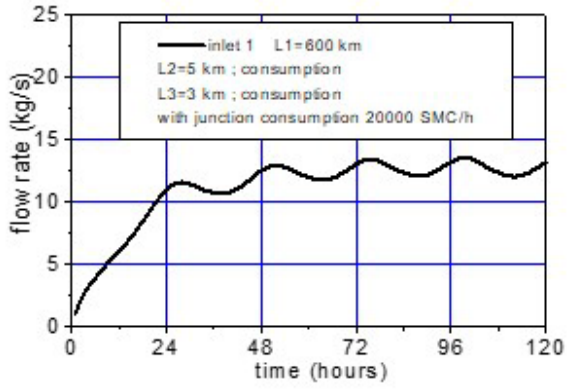

Figure 15. Flow Rate at Inlet Versus Time

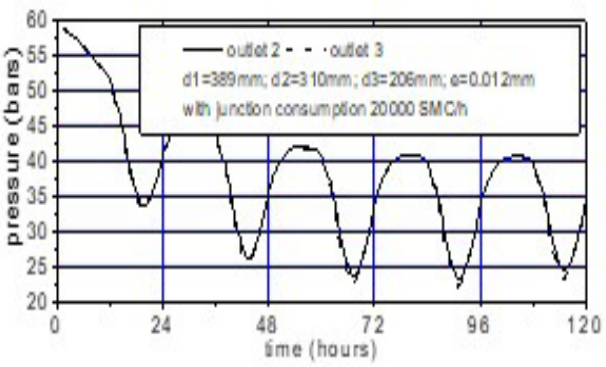

Figure 16. Periodic Pressure at Outlet

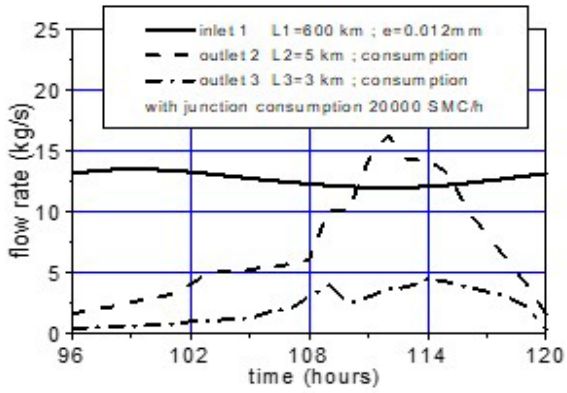

Figure 17. Flow Rate of Periodic Regime Versus Time

4.3.2. Case of Two Consumptions and Two Supplies

We have two power supplies with the same pressure p = 45 bars and two consumptions as shown in thefigure 18. Flows at consumption points are given during 24 hours in NCM/h see (Figure 19).

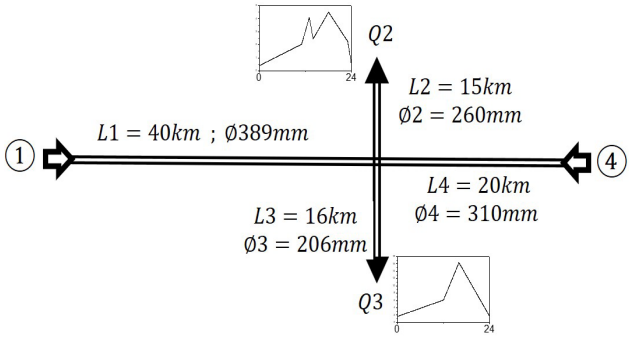

Figure 18. Two Consumptions and Two Supply

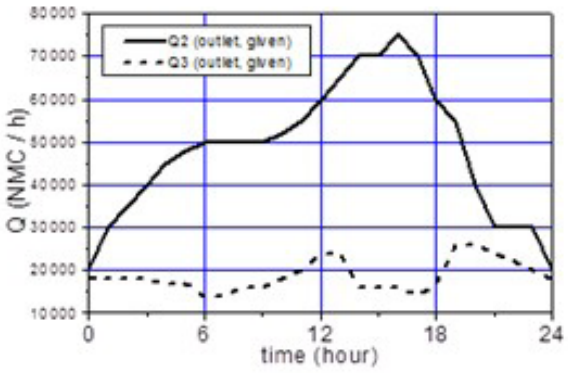

Figure 19. Two Consumptions Given

The initial solution starts from rest. After execution of the computer code, the periodic regime is obtained after6 hours, real time of start-up with the real initial conditions. The flow rates at supply points are shown in the (Figure 20). Note that the flow from the supply point ④ is negative in the calculations; the direction of the flow is taken to be directed to the right (Figure 21).

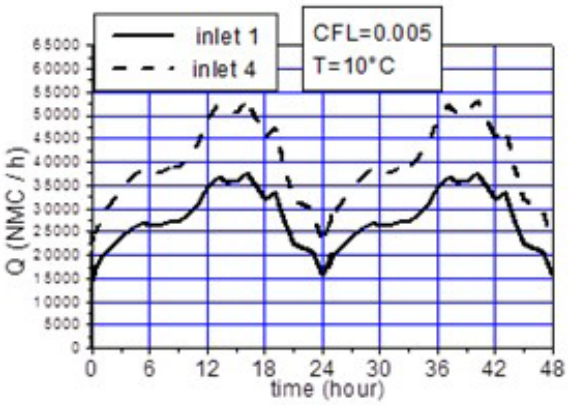

Figure 20. Flow Rate at Two Inlets in Periodic Regime

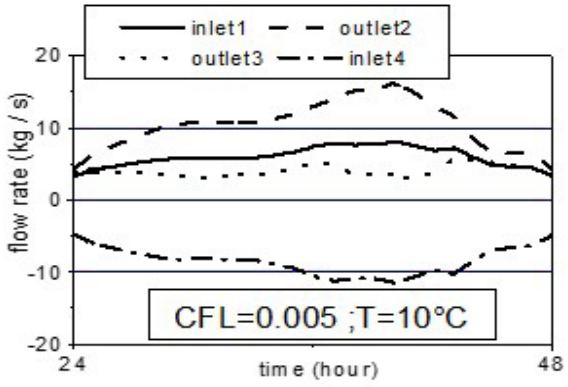

Figure 21. Flow Rate at Inlets and Outlets

The velocity at inlets and outlets of pipe is shown at (Figure 22). We can see that the velocity at inlet ④ is negative.

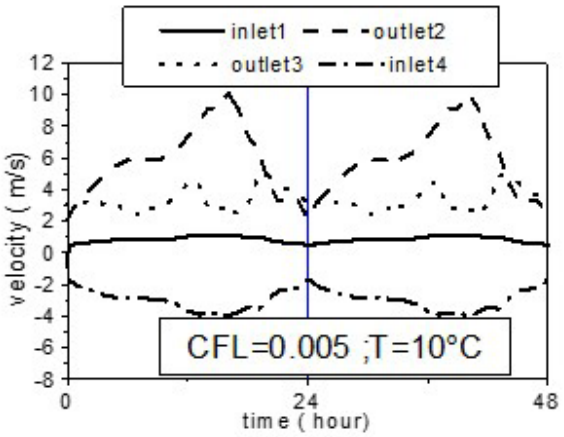

Figure 22. Velocities at Inlets and Outlets

Concerning the variation of the pressure at the points of consumption, are presented in the (Figure 23), we noticed that the pressures obtained are the same with a $CFL = 0.4$ while the convergence of the flows requires a $CFL = 0.005$ (Figure 24).

The Runtime is 36 minutes for $CFL = 0.005$ and $CPU = 1.67\ 10^{-6}{}_{s}$ / (it.mesh).

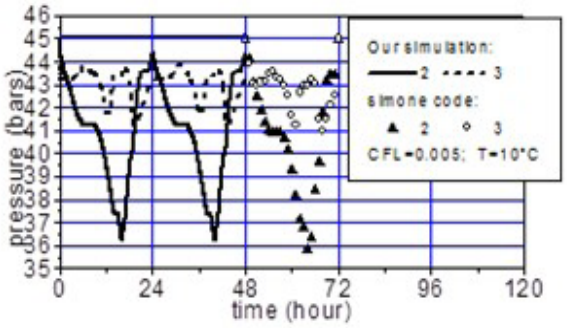

Figure 23. Results with Comparison

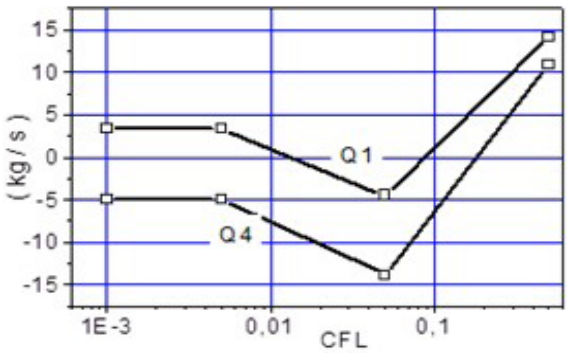

Figure 24. Effect of CFL on the Convergence

Conclusion

The finite difference method remains a good approximation for determining the behavior of the flow in a gas pipeline, the determination of the capacities in each section of the network, and the determination of the supply flow for variable or non-variable consumptions or pressures at the outlet of each section. In the case of a periodic dynamic regime, the computation time is a real parameter, on the other hand in the case of a static regime; the time is an iterative parameter. The choice of the CFL value and the spatial step Δx plays a decisive role in the convergence of the computer code. For the dynamic regime it was observed that the results do not change when the periodic regime is reached, which confirms the consistency of the numerical method. The initial solution does not influence the periodic mode but the transitory solution can take more or less time. The conservation of flows between the inlets and outlets of the pipes is confirmed in the period. We took into account the variation of the compressibility factor and the pressure drop coefficient along the pipes. A comparison was presented with the results obtained by Simone's code. The calculation at the level of the junction points is very delicate and requires a particular discretization of the conservation equations. It is clear that for 24 hours the sum of the flow rates entering equals the sum of the flow rates leaving the pipes. This result is more than sufficient to test that a calculation code is consistent and the calculations are precise.

References

Farzaneh-Gord. M et al, 2016. "Unsteady natural gas flow within pipeline network, an analytical approach" (2016) pp. 398-409. DOI:10.1016/j.jngse.2015.12.017

Hofer. P,1973."Beurteilung von fehlern in rohrnetzberechnungen", gwf-gas/erdgas, vol. 114, no. 3, 1973.

Klaus A. Hoffmann et al, 1995. "Computational Fluid Dynamics for Engineers". Volume II; March 1995.

Ouyang. L. B et al, 1996. "Steady-state gas flow in pipes". Journal of Petroleum Science and Engineering 14 (1996) pp137-158.

Pambour. K. A et al, 2015. "An integrated transient Model for simulating the Operation of Natural Gas Transport Systems". Journal of Natural Gas Science and engineering (2015).

Pascal. H, 1972. "Ecoulement non permanent dans les gazoducs". Editions Technip. (1972).

WangHai et al, (2011)."Transient flow simulation of municipal gas pipelines and networks using semi implicit finite volume method". Science Direct, 12(2011)217-223, doi:10.1016/j.proeng.2011.05.034.

Shanbi. P et al, (2013). "The simulation of Natural Gas Gathering Pipeline Network". The Open Fuels & Energy Science Journal, 2013, 6, 18-22.

JOURNAL OF GAS TECHNOLOGY

Volume 8 / Issue 1 / Summer 2023 / Pages 15-24

Journal Home page: http://jgt.irangi.org

Probing Methane Adsorption in MIL Metal-Organic Frameworks using Molecular Dynamics Simulations

Saman Banijamali[1], Hedayat Azizpour[2*], Parissa Khadiv-parsi[2]

1. M.Sc. Student, School of Chemical Engineering, College of Engineering, University of Tehran, Tehran 11155/4563, Iran
2. Assistant Professor, School of Chemical Engineering, College of Engineering, University of Tehran, Tehran 11155/4563, Iran

ARTICLE INFO

ORIGINAL RESEARCH ARTICLE

Article History:
Received: 29 May 2023
Revised: 24 July 2023
Accepted: 20 August 2023

Keywords:
Metal-organic framework (MOF)
Methane adsorption
Adsorbed Natural Gas Technology (ANG)
Molecular Dynamics Simulation
Monte Carlo Simulation

DOR: 20.1001.1/JGT.2024.2015403.1030

ABSTRACT

In this study, we investigated the adsorption properties of three metal-organic frameworks (MOFs): MIL-101(Cr), MIL-100(Fe), and MIL-100(Al), for high-pressure methane storage in Adsorbed Natural Gas (ANG) applications. Utilizing the Materials Studio software and Monte Carlo simulations, we conducted molecular dynamics simulations under a constant pressure of 35 atm and a temperature of 300 K. The results revealed distinct methane adsorption capacities for each MOF, with values of 0.008 g, 0.089 g, and 0.035 g of methane per gram of adsorbent for MIL-101(Cr), MIL-100(Fe), and MIL-100(Al), respectively. To validate our findings, we compared the calculated adsorption capacity of MIL-101(Cr) with experimental data, resulting in a close match with the reported value of 0.036 g of methane per gram of absorbent. The simulations also unveiled insights into the adsorption patterns, demonstrating that methane molecules selectively interacted with different regions of the frameworks based on their orientation. Our study suggests that MOFs hold promise as suitable adsorbents for natural gas storage in ANG technologies. Among the three studied MOFs, MIL-100(Al) emerged as the most efficient option, presenting potential for future industrial-scale implementation, subject to economic and production considerations. These results further emphasize the significance of nanomaterials, particularly MOFs, in advancing ANG development and highlight the importance of validation with experimental data to ensure accuracy and reliability.

How to cite this article
S. Banijamali, H. Azizpour, P. Khadiv-pars, Probing Methane Adsorption in MIL Metal-Organic Frameworks using Molecular Dynamics Simulations. Journal of Gas Technology. 2023; 8(1): 15 -24. (http://jgt.irangi.org/article_712120.html)

* Corresponding author.
E-mail address: h.azizpour@ut.ac.ir, (H. Azizpour).

Available online 20 September 2023

1. Introduction

Natural gas is a mixture that contains 70-90% methane by volume. Due to factors such as high-octane number, clean combustion, reduced engine maintenance costs, and low pollution levels, it has been able to establish itself as a fuel in the world. The increasing threat of global warming due to the emission of harmful greenhouse gases has prompted interest in clean energy research. Methane (CH_4) has the ability to replace hydrocarbon-based fuels such as oil due to its maximum H to C ratio. Natural gas transportation is generally done in its liquid form. Conventionally, there are three different methods for storing natural gas, which are (1) compressed natural gas (CNG), (2) liquefied natural gas (LNG), and (3) adsorbed natural gas (ANG). The traditional method of storing and maintaining natural gas in vehicles involves using heavy steel tanks under pressure of about 220 atmospheres, which, in addition to being bulky, also has safety issues (Rasoulzadeh et al.,2008; Miana et al.,2010; Mokhatab et al.,2015; Wang,2022).

There are many MOFs (Metal-Organic Frameworks) that have been studied for ANG (Adsorbed Natural Gas) storage, and new materials are always being developed and tested. Some of the important factors when evaluating MOFs for ANG storage include: Methane adsorption capacity: This is the amount of methane that a MOF can adsorb at a specific temperature and pressure. The higher the adsorption capacity, the more methane a MOF can store. Selectivity: This refers to a MOF's ability to preferentially adsorb methane over other gases, such as carbon dioxide or nitrogen. A MOF with high selectivity for methane is desirable for ANG storage because it minimizes the number of other gases adsorbed and maximizes the amount of methane stored. Stability: MOFs must be stable under ANG storage conditions, which may involve high pressures and temperatures. They must also be resistant to degradation over time. Reproducibility: MOFs must be able to effectively release the adsorbed methane and be easily regenerated for reuse. Cost and availability: MOFs must be economically feasible and readily available in large quantities. Pore size and structure: The pore size and structure of MOFs can affect their methane adsorption capacity and selectivity. MOFs with larger pores may have a higher methane adsorption capacity but may also have lower selectivity for methane relative to other gases. Kinetics: The rate at which methane can be adsorbed and desorbed by MOFs is an important consideration for ANG storage, especially during filling and emptying cycles. Compatibility with other materials: MOFs must be compatible with other materials used in ANG storage systems such as tanks, pipelines, and valves. This can affect the overall performance and efficiency of the system. Scalability: MOFs must be scalable for commercial production and integration into ANG storage systems. Safety: MOFs must be safe for handling and use and should not pose risks such as explosion or other hazards. Ultimately, the best MOF for ANG storage depends on various factors such as the specific application and operational conditions. Researchers continue to study and develop new MOFs and optimize existing ones to improve their performance for ANG storage (Davarpanah and Mirshekari,2019; Dang et al.,2020; Wu et al.,2021; Cai et al.,2023; Mergenthal et al.,2023; Wu et al.,2023; Zhang et al.,2023a; Zhang et al.,2023b).

In addition to these factors, it should be noted that MOFs are just one of several materials under investigation for ANG storage. Other materials include activated carbons, porous polymers, and zeolites. The optimal materials for ANG storage depend on various factors, and research continues to identify the most effective and efficient materials for this application (Tagliabue et al.,2009; Alhasan et al.,2016; He et al.,2019; Mahmoud et al.,2019; Bhattacharjee et al.,2020; Reza et al.,2020; Pérez-Botella et al.,2022).

Kinetics is an important factor in evaluating the suitability of adsorbents for ANG storage, as

the rate of methane adsorption and desorption by adsorbents can affect the overall efficiency of the storage system. The kinetics of gas adsorption and desorption depends on factors such as temperature, pressure, and the properties of the gas and adsorbents (Bhattacharjee et al.,2020; Nikravesh et al.,2023).

In ANG storage systems, kinetics can affect the filling and emptying time of the storage tanks. An adsorbent with slow kinetics may require longer filling and emptying times, which can increase the overall time and energy required for filling and emptying the tank. On the other hand, an adsorbent with fast kinetics may provide faster filling and emptying times, which can improve the overall efficiency of the storage system. Several studies have investigated the kinetics of methane adsorption and desorption by MOFs. One approach involves using gravimetric methods to measure the amount of gas absorbed or desorbed as a function of time. Another method involves using pressure measurement techniques to monitor pressure changes during gas adsorption or desorption (Ceglarska-Stefańska and Zarębska,2002; Busch et al.,2004; Gao et al.,2020; Ursueguia et al.,2020).

There are multiple factors that can influence the gas absorption and desorption kinetics by MOFs, including:

Temperature: Higher temperatures generally lead to faster kinetics, but they may also reduce the methane adsorption capacity of MOFs. Pressure: Higher pressures can increase the methane adsorption capacity of MOFs and also lead to faster kinetics. However, it may also require more energy for filling and discharging the storage vessel. Pore size and structure: The size and structure of MOF pores can influence gas adsorption and desorption kinetics. MOFs with larger pores may exhibit faster kinetics, but they might have lower selectivity for methane. MOF properties: MOF properties, such as surface area, pore volume, and surface chemistry, can also affect gas adsorption and desorption kinetics.

Several methods have been used to study gas adsorption and desorption kinetics by MOFs, including gravimetric techniques, pressure measurement techniques, and spectroscopic methods. These studies can provide valuable insights into the factors influencing gas adsorption and desorption kinetics and can assist researchers in optimizing MOFs for ANG storage applications. Overall, gas adsorption and desorption kinetics are crucial considerations when evaluating MOFs for ANG storage, and optimizing this kinetics can improve the efficiency of ANG storage systems (Ceglarska-Stefańska and Zarębska,2002; Busch et al.,2004; Teo et al.,2017; Gao et al.,2020; Ursueguia et al.,2020)

Until now, various porous materials, such as silica gel, activated carbon, carbon nanotubes, zeolites, and covalent-organic and metal-organic frameworks (MOFs), have been experimentally investigated for ANG (Adsorbed Natural Gas) applications. The classical method for surface adsorption studies involves the synthesis or acquisition of raw materials, designing and implementing the adsorption process, and finally conducting device experiments for characterization and measurement of the adsorption capacity. Considering the costs of raw materials and the required facilities, especially in high-pressure processes, the importance of computational and simulation methods has become more pronounced. One common approach is molecular dynamics simulation, a numerical method used to solve Newton's equations of motion for individual particles in a system. Due to the advantages of metal-organic frameworks for methane storage, research in this area has recently increased. Among the most important metal-organic frameworks used in these studies is the MIL family, known for its high porosity, suitable pore size, and favorable intermolecular interactions, resulting in significant methane adsorption capacity. For instance, Kayal et al. (2016) obtained an approximate methane adsorption of 0.25-0.5 kg of methane per kilogram of adsorbent at 600

kilopascals using Monte Carlo simulations, which was in line with experimental findings. Zhang et al. (2019) calculated methane adsorption to be around 125 molecules per large hexagonal pore and about 50 molecules per small pentagonal pore of MOFs, using different computational methods (Bimbo et al.,2021) reported an average methane enthalpy of adsorption of 13.5 kJ/mol for the specific framework. In a study conducted by Zhao et al. (2020) the isosteric heat of methane adsorption on this framework was found to be 22.94 kJ/mol (Furukawa and Yaghi,2009; Zhu and Zhao,2014; Bimbo et al.,2021; Moradi et al.,2021; Moradi et al.,2022)

In this study, methane adsorption on metal-organic frameworks MIL-101(Cr), MIL-100(Fe), and MIL-100(Al) was simulated using the DS BIOVIA Materials Studio 2017 software.

2. Methods And Materials

In this study, three different metal-organic frameworks (MOFs) were chosen for methane adsorption simulations: MIL-101(Cr), MIL-100(Fe), and MIL-100(Al). MOFs are a class of highly porous materials with a high surface area, making them promising candidates for gas storage and separation applications. MIL-101(Cr) was characterized with a surface area of 2600 m^2/g, which makes it particularly attractive for gas storage purposes.

2.1.Crystal Structure Optimization

Before performing the simulations, the crystal structure of each MOF was optimized for use in the molecular dynamics simulation software. This optimization involved considering the atomic ratios, bond types, hydrogen atoms in the structure, and framework energies using the Compass force field and the atom-based summation method. The Compass force field is a widely used force field for organic and inorganic materials, and the atom-based summation method is utilized to efficiently compute interactions between atoms in the system.

The equations used in computational chemistry for geometry optimization with a force field involve calculating the potential energy of the system and the forces acting on each atom. One common form of the potential energy equation used in molecular mechanics force fields is the following:

$$Etotal=\sum bondskr(r-req)2+\sum angleskθ(θ-θeq)2+\sum torsions2Vn(1+cos(nϕ-γ))+\sum non\text{-}bonded(r12A-r6B)+\sum electrostatic4πϵ0rijqiqj \quad (1)$$

Where:

E_{total} is the total potential energy of the system.

K_r and r_{eq} are the force constant and equilibrium bond length for each bond.

k_θ and θ_{eq} are the force constant and equilibrium angle for each angle.

Vn, n, and γ are parameters describing torsional rotations.

A and B are parameters for the Lennard-Jones potential describing van der Waals interactions.

q_i and q_j are the charges on atoms i and j, and r_{ij} is the distance between them, for electrostatic interactions. (Sun,1998).

2.2.Methane Molecule Optimization

In order to represent the methane molecule accurately in the simulation, it was drawn and optimized using the graphical tool provided by the DS BIOVIA Materials Studio 2017 software. This optimization ensures that the geometry and bond lengths of the methane molecule are at their most stable configuration, which is essential for reliable simulations. Equations for methane optmizations are same as (eq.1).

2.3.Simulation Setup

The simulations were carried out using the adsorption and molecular dynamics modules of the software. The Universal force field, which is a general-purpose force field suitable for organic and inorganic systems, was employed to model the interactions between methane molecules and the MOFs. The Ewald summation method

was used to handle the long-range electrostatic interactions between charged species in the system, providing accurate energy calculations.

2.4. Sorption and Forcite Modules

The Sorption module was used to perform adsorption simulations, where methane molecules were introduced into the MOF structures to investigate their adsorption behavior at different temperatures and pressures. The forcite module was utilized for molecular dynamics simulations, which allowed the investigation of the dynamic behavior of methane molecules within the MOFs over time.

The equations used in forcite for molecular dynamics simulations involve calculating forces and energies associated with bonded and non-bonded interactions. Here's an overview of the equations:

Bended interactions:

$$Bond\ stretching: E_{\text{bond}} = \frac{1}{2} k_{bond} (r - \text{req})^2 \quad (2)$$

$$Angle\ bending: E_{angle} = \frac{1}{2} K_{angle} (\theta - \theta eq)^2 \quad (3)$$

Here, k_{bond} and K_{angle} are force constants, r is the bond length, r_{eq} is the equilibrium bond length, θ is the bond angle, and θ_{eq} is the equilibrium bond angle.

For dihedral or torsional terms, Forcite typically uses a Fourier expansion:

$$E_{dihedral} = \sum_{n=1}^{N} Vn[1 + cos(n\phi - \gamma)] \quad (4)$$

Here, Vn are the Fourier coefficients and γ represents the phase angle.

In Forcite simulations, typically, Lennard-Jones (van der Waals) and Coulomb (electrostatic) interactions are considered as non-bonded interactions. However, in this case, we assume the absence of charged molecules and ions, rendering Coulomb interactions negligible.

$$E_{LJ} = \sum_{i<j} 4\,\epsilon_{ij} \left[\left(\frac{rij}{\sigma ij} \right)^{12} - \left(\frac{rij}{\sigma ij} \right)^{6} \right] \quad (5)$$

Here, ϵ_{ij} is the depth of the potential well, σ_{ij} is the finite distance at which the inter-particle potential is zero, q_i and q_j are the charges, and r_{ij} is the distance between particles i and j (Shankar et al.,2022).

2.5. Experimental Parameters

In molecular dynamics simulations, a molecular system is described with various parameters, including the volume and temperature. These parameters are crucial for understanding the behavior of gases in porous materials. The volume of the simulation cell influences the amount of gas that can be adsorbed, and the temperature affects the kinetic energy and motion of the molecules. Volume of each was obtained from crystallography open database and assumption for temperature was 298 K.

2.6. Force Field Analysis

After conducting the simulations, the Force Field Analysis tool was used to calculate and plot the concentration profile and adsorption capacity of methane within the MOFs. This analysis provided insights into the distribution and uptake of methane molecules at different temperatures and pressures (Zhao et al.,2020; Frenkel and Smit,2023).

3. Results and Discussion

In this study, surface adsorption of methane on the MIL-101(Cr) MOF was simulated under a constant pressure of 35 atmospheres and a temperature of 300 K, using a total of 140,000-time steps, each lasting 1 femtosecond. The reason for choosing this temperature and pressure is to replicate the conditions used in Kayal et al.'s research to ensure accurate simulation with the optimized force field.

In Kayal's research, the methane adsorption capacity for these conditions in the MIL-101(Cr) MOF was reported (He et al.,2019).

By using simulations with different force fields, the optimal force field can be determined. The adsorption levels at different time intervals are shown in (Figure 2). As observed, shortly after starting, the system reaches equilibrium and adsorbs 1435 methane molecules per cell. With simple multiplication and division calculations and having information about the density, temperature, pressure, and crystal size used in the simulation, this value is calculated as 0.035 kg of methane per kilogram of MOF.

According to Kayal et al.'s research (2016), this value was experimentally determined and reported as 0.036 kg of methane per kilogram of MOF. The difference between the simulation and experimental values (about 5.5%) can be attributed to various factors, such as experimental errors, truncation errors in numerical calculations, limited time intervals in the simulation, and the choice of force field (He et al.,2019; Frenkel and Smit,2023).

Other adsorption values obtained through similar calculations are listed in (Table 1).

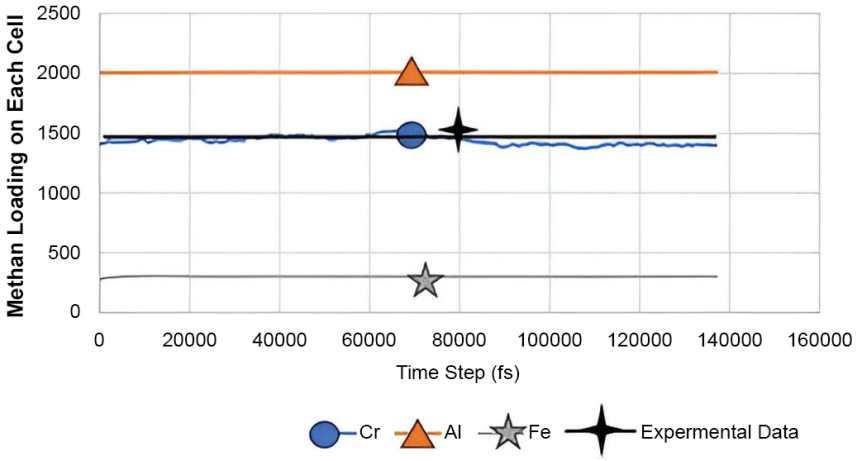

Figure 1. Methane Loading on each Simulation Cell for Different MOFs during Time

Table 1. Result of Simulation on Different MOFs

MOF	Adsorbed molecule per cell	Mass of each cell (amu)	Loading (g/g)
MIL-100(Fe)	303	236156	0.008
MIL-100(Al)	2007	14039	0.089
MIL-101(Cr)	1461	264256	0.035

(Figure 2) illustrates the adsorption fields in the MIL-101(Cr) MOF. The blue points indicate stronger adsorption fields, and the color intensity represents the strength of the adsorption field. These figures demonstrate that methane adsorption and storage occur throughout the MOF, including in both pentagonal and hexagonal cavities, as well as near the linker and cluster connection points or the center of empty cavities.

In the methane molecule, partial positive charges reside on the hydrogen atoms, while partial negative charges are present on the carbon atom. The orientation of methane molecules trapped in the framework varies depending on their location. Methane is adsorbed from its carbon part near the hydrogen and chromium atoms in the framework, and it is adsorbed from its hydrogen part near the oxygen atoms. Considering that methane

contains more hydrogen atoms, it is logical to have stronger adsorption fields (highlighted regions in Figure 2) around the oxygen atoms.

Finally, (Figure 3) represents the adsorption profile at different distances from the framework. The left side of the simulation cell is set as the center coordinates, and the cell width is divided into 10 equal parts. The concentrations are given as averages in the z-direction relative to the lowest concentration. Therefore, the concentration reaches its maximum value in the middle of the framework, indicating the convergence of equations towards equilibrium. By using larger time steps in the simulation, more accurate and close-to-real results can be achieved.

It's important to note that relative concentration refers to the ratio of the absorbed gas concentration within the framework to the concentration of the gas not absorbed in the surrounding vicinity of the framework. The variance in adsorption across different frameworks within the MOF family can be attributed to the interaction between methane and metal clusters, as well as differences in cavity dimensions. To clarify, relative concentration signifies the quantity of gas absorbed within the framework compared to the amount of gas present in the surrounding area outside the framework.Overall, these simulations provide valuable insights into the adsorption behavior of methane in the MIL-101(Cr) MOF and help us understand the interaction between methane molecules and the MOF structure.

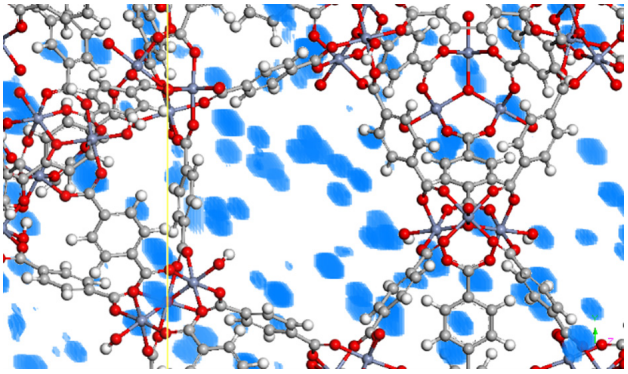

Figure 2. Adsorption Field in MOF. The Intensity of Colors Indicates the Strength of the Fields

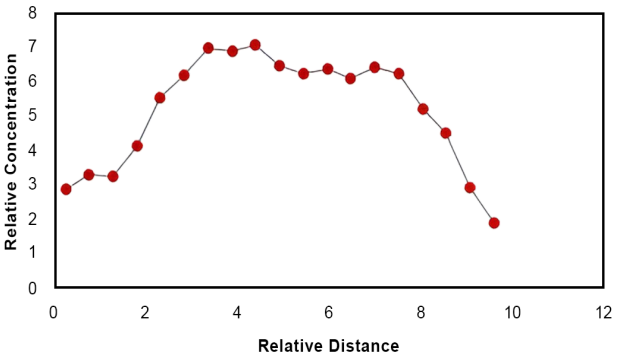

Figure 3. The Concentration Profile of Methane Adsorption for MIL-101(Cr) at the end of the Simulation Time

4. Conclusions

The three metal-organic frameworks (MOFs) and methane structures were placed together in the Materials Studio software, and intermolecular interactions were calculated for each of them at a pressure of 35 atmospheres and a temperature of 300 K using the Universal force field. According to the simulation results, adsorption amounts of 0.008 g, 0.089 g, and 0.035 g of methane per gram of absorbent were obtained for the clusters with iron, aluminum, and chromium cores, respectively. To verify the obtained values, another research that experimentally calculated the adsorption amount on the chromium core framework under the same conditions and found 0.036 g of methane per gram of absorbent was used. Considering the acceptable range of adsorption amounts for various practical adsorbents in ANG technology, such as activated carbon and zeolites, it can be said that the studied MOFs are suitable frameworks for gas adsorption and storage. Among these frameworks, MIL-100(Al) proves to be the best option, and if its industrial-scale production is feasible, it can be used as an adsorbent in ANG. It is worth noting that this research and similar studies indicate the technical efficiency of metal-organic frameworks. However, the hindrance to their practical application lies in economic and mass production considerations, which can be addressed with the growth of relevant technologies. In conclusion, metal-organic

frameworks have shown promise as efficient adsorbents for natural gas storage in ANG applications. The development of these frameworks may be limited by economic and production factors, but with advancing technologies, their practical application can be improved.

References

Alhasan, S., R. Carriveau and D.-K. Ting (2016). "A review of adsorbed natural gas storage technologies." International Journal of Environmental Studies 73(3): 343-356. https://doi.org/10.1080/00207233.2016.1165476

Bhattacharjee, G., H. P. Veluswamy, R. Kumar and P. Linga (2020). "Rapid methane storage via sII hydrates at ambient temperature." Applied Energy 269: 115142. https://doi.org/10.1016/j.apenergy.2020.115142

Bimbo, N., J. P. Smith, H. Aggarwal, A. J. Physick, A. Pugsley, L. J. Barbour, V. P. Ting and T. J. Mays (2021). "Kinetics and enthalpies of methane adsorption in microporous materials AX-21, MIL-101 (Cr) and TE7." Chemical Engineering Research and Design 169: 153-164. https://doi.org/10.1016/j.cherd.2021.03.003

Busch, A., Y. Gensterblum, B. M. Krooss and R. Littke (2004). "Methane and carbon dioxide adsorption-diffusion experiments on coal: upscaling and modeling." International Journal of Coal Geology 60(2-4): 151-168. https://doi.org/10.1016/j.coal.2004.05.002

Cai, Y., H. Chen, P. Liu, J. Chen, H. Xu, T. Alshahrani, L. Li, B. Chen and J. Gao (2023). "Robust microporous hydrogen- bonded organic framework for highly selective purification of methane from natural gas." Microporous and Mesoporous Materials 352: 112495. https://doi.org/10.1016/j.micromeso.2023.112495

Ceglarska-Stefańska, G. and K. Zarębska (2002). "The competitive sorption of CO_2 and CH_4 with regard to the release of methane from coal." Fuel Processing Technology 77: 423-429. https://doi.org/10.1016/S0378-3820(02)00093-0

Dang, W., J. Zhang, H. Nie, F. Wang, X. Tang, N. Wu, Q. Chen, X. Wei and R. Wang (2020). "Isotherms, thermodynamics and kinetics of methane-shale adsorption pair under supercritical condition: Implications for understanding the nature of shale gas adsorption process." Chemical Engineering Journal 383: 123191. https://doi.org/10.1016/j.cej.2019.123191

Davarpanah, A. and B. Mirshekari (2019). "Experimental investigation and mathematical modeling of gas diffusivity by carbon dioxide and methane kinetic adsorption." Industrial & Engineering Chemistry Research 58(27): 12392-12400. https://doi.org/10.1021/acs.iecr.9b01920

Frenkel, D. and B. Smit (2023). Understanding molecular simulation: from algorithms to applications, Elsevier.0323913180,

Furukawa, H. and O. M. Yaghi (2009). "Storage of hydrogen, methane, and carbon dioxide in highly porous covalent organic frameworks for clean energy applications." Journal of the American Chemical Society 131(25): 8875-8883. https://doi.org/10.1021/ja9015765

Gao, Z., D. Ma, Y. Chen, C. Zheng and J. Teng (2020). "Study for the effect of temperature on methane desorption based on thermodynamics and kinetics." ACS omega 6(1): 702-714. https://doi.org/10.1021/acsomega.0c05236

He, Z., K. Zhang and J. Jiang (2019). "Formation of CH4 hydrate in a mesoporous metal-organic framework MIL-101: Mechanistic insights from microsecond molecular dynamics simulations." The journal of physical chemistry letters 10(22): 7002-7008. https://doi.org/10.1021/acs.jpclett.9b02808

Mahmoud, E., L. Ali, A. El Sayah, S. A. Alkhatib, H. Abdulsalam, M. Juma and A. a. H. Al-Muhtaseb (2019). "Implementing metal-organic frameworks for natural gas storage."

Crystals 9(8): 406. https://doi.org/10.3390/cryst9080406

Mergenthal, M., A. Tawai, S. Amornraksa, S. Roddecha and S. Chuetor (2023). "Methane enrichment for biogas purification using pressure swing adsorption techniques." Materials Today: Proceedings 72: 2915-2920. https://doi.org/10.1016/j.matpr.2022.08.003

Miana, M., R. Del Hoyo, V. Rodrigálvarez, J. R. Valdés and R. Llorens (2010). "Calculation models for prediction of Liquefied Natural Gas (LNG) ageing during ship transportation." Applied Energy 87(5): 1687-1700. https://doi.org/10.1016/j.apenergy.2009.10.023

Mokhatab, S., W. A. Poe and J. Mak (2015). "Chapter 1-natural gas fundamentals." Handbook of Natural Gas Transmission and Processing, 3rd ed.; Gulf Professional Publishing: Boston, MA, USA: 1-36. https://doi.org/10.1016/B978-0-12-801499-8.00001-8.

Moradi, H., H. Azizpour, H. Bahmanyar and M. Emamian (2022). "Molecular dynamic simulation of carbon dioxide, methane, and nitrogen adsorption on Faujasite zeolite." Chinese Journal of Chemical Engineering 43:70-76. https://doi.org/10.1016/j.cjche.2021.05.034

Moradi, H., H. Azizpour, H. Bahmanyar, N. Rezamandi and P. Zahedi (2021). "Effect of Si/Al ratio in the faujasite structure on adsorption of methane and nitrogen: a molecular dynamics study." Chemical Engineering & Technology 44(7): 1221-1226. https://doi.org/10.1002/ceat.202000356

Nikravesh, N. Y., M. Beygzadeh and M. Adl (2023). "Microporous MOF-5@ AC and Cu-BDC@ AC Composite Materials for Methane Storage in ANG Technology." International Journal of Energy Research 2023. https://doi.org/10.1155/2023/2282746

Pérez-Botella, E., S. Valencia and F. Rey (2022). "Zeolites in adsorption processes: State of the art and future prospects." Chemical Reviews 122(24): 17647-17695. https://doi.org/10.1021/acs.chemrev.2c00140

Rasoulzadeh, M., S. Fatemi, H. M. GHOLAM and M. Mousavian (2008). "Study of methane storage and adsorption equilibria in multi-walled carbon nanotubes." https://doi.org/10.30492/ijcce.2008.6977

Reza, M. S., C. S. Yun, S. Afroze, N. Radenahmad, M. S. A. Bakar, R. Saidur, J. Taweekun and A. K. Azad (2020). "Preparation of activated carbon from biomass and its' applications in water and gas purification, a review." Arab Journal of Basic and Applied Sciences 27(1): 208-238. https://doi.org/10.1080/25765299.2020.1766799

Shankar, U., R. Gogoi, S. K. Sethi and A. Verma (2022). Introduction to Materials Studio Software for the Atomistic-Scale Simulations. Forcefields for Atomistic-Scale Simulations: Materials and Applications, Springer: 299-313,

Sun, H. (1998). "COMPASS: An ab Initio Force-Field Optimized for Condensed-Phase ApplicationsOverview with Details on Alkane and Benzene Compounds." The Journal of Physical Chemistry B 102(38): 7338-7364.10.1021/jp980939v

Tagliabue, M., D. Farrusseng, S. Valencia, S. Aguado, U. Ravon, C. Rizzo, A. Corma and C. Mirodatos (2009). "Natural gas treating by selective adsorption: Material science and chemical engineering interplay." Chemical Engineering Journal 155(3): 553-566. https://doi.org/10.1016/j.cej.2009.09.010

Teo, H. W. B., A. Chakraborty and S. Kayal (2017). "Evaluation of CH_4 and CO_2 adsorption on HKUST-1 and MIL-101 (Cr) MOFs employing Monte Carlo simulation and comparison with experimental data." Applied Thermal Engineering 110: 891-900. https://doi.org/10.1016/j.applthermaleng.2016.08.126

Ursueguia, D., E. Diaz and S. Ordonez (2020). "Adsorption of methane and nitrogen on Basolite MOFs: Equilibrium and kinetic studies." Microporous and Mesoporous Materials

298: 110048. https://doi.org/10.1016/j.micromeso.2020.110048

Wang, Q. (2022). Surface Process, Transportation, and Storage, Elsevier.0128242086,

Wu, X., Z. Cao, X. Lu and W. Cai (2023). "Prediction of methane adsorption isotherms in metal-organic frameworks by neural network synergistic with classical density functional theory." Chemical Engineering Journal 459: 141612. https://doi.org/10.1016/j.cej.2023.141612

Wu, Z., V. Wee, X. Ma and D. Zhao (2021). "Adsorbed natural gas storage for onboard applications." Advanced Sustainable Systems 5(4): 2000200. https://doi.org/10.1002/adsu.202000200

Zhang, G., Z. Liu, Y. Kong and F. Wang (2023a). "Hydrate-based adsorption-hydration hybrid approach enhances methane storage in wet MIL-101 (Cr)@ AC under mild condition." Chemical Engineering Journal 472: 145068. https://doi.org/10.1016/j.cej.2023.145068

Zhang, Q., X. Lian, R. Krishna, S.-Q. Yang and T.-L. Hu (2023b). "An ultramicroporous metal-organic framework based on octahedral-like cages showing high-selective methane purification from a six-component C1/C2/C3 hydrocarbons mixture." Separation and Purification Technology 304: 122312. https://doi.org/10.1016/j.seppur.2022.122312

Zhao, G., Q. Zheng, X. Zhang and W. Zhang (2020). "Adsorption equilibrium and the effect of honeycomb heat exchanging device on charge/discharge characteristic of methane on MIL-101 (Cr) and activated carbon." Chinese Journal of Chemical Engineering 28(7): 1964-1972. https://doi.org/10.1016/j.cjche.2020.04.021

Zhu, X. and Y.-P. Zhao (2014). "Atomic mechanisms and equation of state of methane adsorption in carbon nanopores." The Journal of Physical Chemistry C 118(31): 17737-17744. https://doi.org/10.1021/jp5047003

JOURNAL OF GAS TECHNOLOGY

Volume 8 / Issue 1 / Summer 2023 / Pages 25-34

Journal Home page: http://jgt.irangi.org

A Novel Method for Heat Integration of Natural Gas Sweetening Process

Ehsan Fatehi, Parisa Sadat Fatemi, Mohammad Javad Zarkesh, Mahshid Moradi, Shahab Taleghani, Mahsa Majidi*

Department of Chemical Engineering, Pazhoohesh Institute, Tehran, Iran

ARTICLE INFO

ORIGINAL RESEARCH ARTICLE

Article History:
Received: 26 April 2023
Revised: 18 June 2023
Accepted: 20 August 2023

Keywords:
Natural gas sweetening
Monoethanol-amine
Heat integration
Utility consumption reduction

ABSTRACT

The natural gas sweetening unit usually involves an absorption column and a distillation column. The absorption column completely removes H_2S and CO_2 from natural gas, and the distillation column is used to recover the solvent. The main problem is high energy consumption in the gas sweetening process, particularly in the distillation column, necessitating energy optimization of this process. A novel method was used in this study for heat integration of the natural gas sweetening process. To this end, liquid and vapor streams leaving the absorption column entered the top and bottom of the distillation column, respectively. The feed entering the distillation column was preheated by the bottom product. The liquid and vapor streams reduced the cold and hot utilities of the distillation column, and feed preheating reduced the heat duty of the reboiler. The recycled solvent was then pre-cooled by the sweetened gas. According to the results, the proposed method reduced energy consumption by 67%. Moreover, the proposed process could reduce the total annual cost (TAC) of the base process to the maximum value of 66.7% This reduction in TAC is due to the reduction of operating cost and capital cost by 66.77 and 66.64%, respectively.

DOR: 20.1001.1/JGT.2024.560604.1005

How to cite this article
E. Fatehi, P. Sadat Fatemi, M.J. Zarkesh, M. Moradi, S. Taleghani, M. Majidi, A Novel Method for Heat Integration of Natural Gas Sweetening Process. Journal of Gas Technology. 2023; 8(1): 25 -34. (http://jgt.irangi.org/article_712117.html)

* Corresponding author.
E-mail address: mahsamajidi94@gmail.com, (M. Majidi).

Available online 20 September 2023

1. Introduction

Fossil fuels are the main fountainhead of energy all around the world(Song et al., 2017). Natural gas will be among the most momentous and famed superseded in the coming decades (Baccanelli et al., 2016). Because of its location in profound subbasement reservoirs, natural gas possesses several non-hydrocarbon components, such as carbon and hydrogen sulfide (H_2S) (Seo et al., 2016). These impurities are unwanted components., which may result in the corrosion of materials and environmental problems, such as global warming and acid rain (Chen et al., 2016). These gases may also cause health problems for humans and even death. The elimination of CO_2 from natural gas can effectivelyincreasethe heating value of the final product. (the gas that is sold) and other products (Tavan and Tavan, 2014). Accordingly, the natural gas should be sweetened through various techniques, such as physical absorption, membrane processes, hydrate, cryogenic distillation and absorption using chemical solvents like amines(Mohamadi-Baghmolaei et al., 2021) . Gas sweetening with amine solvents is among the important procedures for removing acid gases (Song et al., 2017).

Amines are organic compounds in which nitrogen is connected to the radical chain. In this regard, one of the most common processes is gas sweetening using alkanolamine solutions. As its name indicates, alkanolamine is considered a mix of alcohol and ammonia(Al Hatmi et al., 2019). The difference between various amines is caused by the different numbers of alcohol radicals replaced with hydrogens of ammonia. Today, monoethanolamine (MEA), diethanolamine (DEA), methyl diethanolamine (MDEA), diglycolamine (DGA), and diisopropanolamine are the most important alkanolamines used in natural gas sweetening units(Kohl and Nielsen, 1997). The MEA is typically used due to its availability, relatively low price, and rapid absorptionThe cost-effectiveness and high handling capacity of large amounts of feed are some of the benefits of amine-based absorption processes. (Song et al., 2017).

Gutierrez et al. used MDEA solution to compare a conventional process of natural gas sweetening with an absorption process using recompressed vapor and a membrane process in terms of compression and pump power, total specific heat, CO_2 removal, CH_4 wastes, and capital cost. The process that used a membrane system consumed lower energy than the other two processes by 77% and 72%, respectively. It also emitted less pollution by 80% and 76%, respectively. However, the overall cost of the membrane system was respectively 12% and 5% more than the capital cost of the other two methods. Moreover, the CH_4 waste in this system was higher than the two other processes(Gutierrez et al., 2017). Mohamadi-Baghmolaei et al. studied different combinations of MDEA and DEA to reduce the exergy loss, energy loss, and CO_2 emission in the gas sweetening process Their outcomes showed that the absorption column and the stripper were accountable for 37% of the total exergy loss and 29% of the energy consumption.

The concentration of DEA plays a crucial role in the exergy and energy management of the natural gas sweetening process. The optimum concentration of amine was found to be 40 wt.%, lowering the total exergy loss from 6.6 MW to 4.8 MW and the energy loss by 36.7%. The CO_2 emission has reached 2893.6 tons per year(Mohamadi-Baghmolaei et al., 2021). Long et al. used heat pump and SHRT methods to propose a novel process for natural gas sweetening with amines. In this process, the latent heat and sensible heat could be circulated using the SHRT method, which resulted in a remarkable improvement in energy efficiency. According to the obtained results, the suggested process could reduce the reboiler duty and operating cost by 62.5% and 45.9%, respectively, compared to a typical gas sweetening process. It also resulted in a 31.2% lower reboiler duty and 22.6% lower

operating cost than the heat pump method (Long and Lee, 2017). Kazmi et al. compared gas sweetening processes with three different solvents, including MEA, DME, and 3MEPYNTF2 (ionic solvent), in terms of exergy, economic and energy, According to the results, the total energy consumed in the three processes equaled 57.45, 30.98, and 13.3 MW, respectively. Moreover, the economic analysis indicated that the ionic solvent led to 83.27% and 73.38% energy saving in TAC in comparison with the other two processes(Kazmi et al., 2021).

Very high energy consumption is the major challenge in the natural gas sweetening process. A large part of energy is consumed in the distillation column where the solvent is recovered. Energy consumption in the whole process was significantly reduced using a novel method. In this method, a liquid stream and a vapor stream leave the absorption column and respectively enter the top and bottom of the distillation column. In this way, part of the heat required in the distillation column is supplied by these two streams, reducing the heat duties of the reboiler and condenser. The feed entering the distillation column is then preheated by the bottom product, and the solvent recycled to the absorption column is precooled by the sweet gas, significantly reducing the hot and cold utilities of the process. The advantage of this method in the natural gas sweetening process, compared to other heat integration techniques like VRC (Gutierrez et al., 2017), heat pump (Long and Lee, 2017), and SHRT(Long and Lee, 2017), lies in its non-reliance on a compressor, which leads to a decrease in process costs. Hence, the proposed method is anticipated to outperform other heat integration strategies.

2. Case Study

This study focused on the natural gas sweeteningprocessthroughmonoethanolamine solvent.

(Table 1) indicates the feed/solvent qualifications.

Table 1. Feed/Solvent Conditions

		Feed		Solven
Temperature (°C)		30		30
Pressure (kPa)		3000		5000
Mass flow rate [kg/h]		75600		100000
Mole fraction	Methane	0.85		
	Ethane	0.04		
	Propane	0.02	H_2O	0.8878
	i-Butane	0.007		
	n-Butane	0.006		
	i-Pentane	0.004		
	n-Pentane	0.003		
	CO_2	0.03		
	H_2S	0.02	MEA	0.1122
	N_2	0.01		
	H_2O	0.01		

It is worth mentioning that feed/solvent qualifications are identical in both processes.

3. Methods

In this research, the Aspen HYSYS V.11 software was utilized for process simulation, and the Modified HYSIM Inside-Out solver was used to run the solver to enhance the precision. In addition, the Acid Gas-Chemical Solvents equation was applied to the fluid package.

3.1. Process Simulation

This paper evaluated the natural gas sweetening by monoethanolamine solvent with and without heat integration.

3.1.1. The Process of Natural Gas Sweetening by Monoethanolamine Solvent Without Heat Integration

The simulation process of natural gas sweetening using monoethanolamine solvent in Aspen HYSYS software is demonstrated in (Figure 1). The feed and solvent enter the absorption column from top and bottom in this figure. The upper and lower pressures of the absorbtion column are 4800 and 4900 kPa, respectively. The top product of the column is sweet gas, and the bottom product is a mixture of solvent and sour gas, which is released from the first column and enters the fifth tray after reaching a temperature of 100 °C. Similarly, the second column consists of 20 trays with 101.3 and 130 kPa pressure on the bottom and top of the column, respectively. The top product of the second column is H_2S and CO_2 and the bottom product contains monoethanolamine and water, which reaches the initial pressure and temperature of the solvent again after passing the pump and cooler and returns to the process beginning.

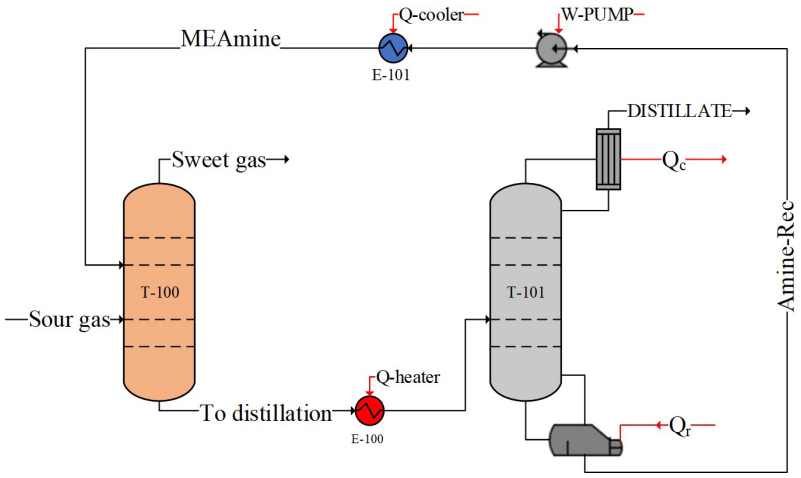

Figure 1. Process of Natural Gas Sweetening using Monoethanolamine Solvent

3.1.2. The Process of Natural Gas Sweetening by Monoethanolamine Solvent with Heat Integration

(Figure 2) depicts the process of natural gas sweetening using monoethanolamine solvent with heat integration in Aspen HYSYS software. The feed and solvent are entered the absorption column from the top and bottom, respectively. The upper and lower pressures of the absorbtion column are 4800 and 4900 kPa, respectively. The top product of the column is sweet gas, and the bottom product is a mixture of solvent and sour gas, which is preheated by the bottom product of the second column. Then, the preheated product is entered into the heater to reach 100°C, finally entering the fifth tray of the second column. Two currents, one in liquid and the other in steam form exit the first column and enter trays 2 and 19 of the second column,

respectively, to minimize the heat duty of the reboiler and condenser. As the prior procedure, the first and second columns contain 20 trays, and the upper and lower pressures of the column are 101 and 130 kPa, respectively. The distillate of the second column (H_2S and CO_2) and the bottom product containing monoethanolamine and water, are pre-cooled by sweet gas released from the top of the first column and reaches 75 °C after gaining a pressure of 5000 kPa. Then, this product is cooled to 30 °C by the cooler and finally returned to the process beginning.

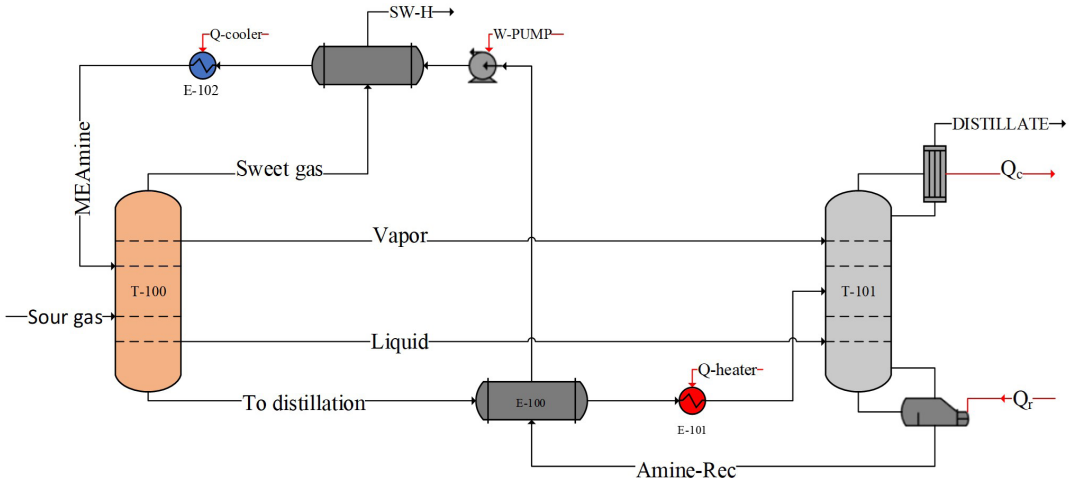

Figure 2. Process of Natural Gas Sweetening using Monoethanolamine Solvent with Heat Integration

3.2. TAC Calculation

In this research, in order to compare the economic cost of the two simulated processes, the parameter of Total Annual Cost (TAC) has been used. The Total Annual Cost is calculated as the sum of the annual operating costs and the annual capital costs. The Total Annual Cost has been calculated through Eq.(1) (Babaie and Esfahany, 2020) In this research, in order to compare the economic cost of the two simulated processes, the parameter of Total Annual Cost (TAC) has been used. The Total Annual Cost is calculated as the sum of the annual operating costs and the annual capital costs. The Total Annual Cost has been calculated through Eq.(1) (Babaie and Esfahany, 2020).

$$TAC = Operating\ Cost + \left(\frac{Capital\ Cost}{Payback\ Period}\right) \quad (1)$$

This paper considers a payback period of 5 years and a man-hour value of 2480 hours. Further information regarding the economic analysis can be found in Appendix A (Babaie and Esfahany, 2022).

4. Results and Discussion

The heat duty of the reboiler and condenser in the two mentioned processes is indicated in (Table 2).

Table 2. Heat Duty of the Reboiler and Condensers

Heat Duty [MW]	P1	P1
Q_r	88040	29240
Q_c	88020	29240
Q-heater	3.053	0.8145
Q-cooler	8.747	4.69
W-pump	0.1882	0.1852

Q_c and Q_r represent the heat duty of the second column's condenser and reboiler, respectively. In addition, Q-heater, Q-cooler, and W-pump show the heat duty of the heater, cooler, and pump power, respectively.

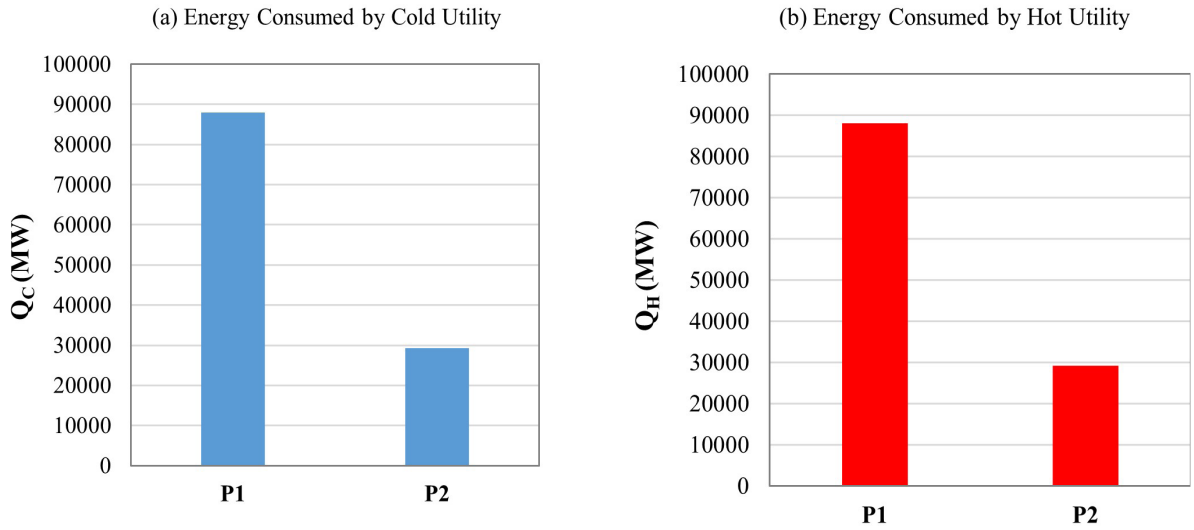

Figure 3. Comparing the Energy Consumption (a) Energy Consumed by Cold Utility, (b) Energy Consumed by Hot Utility

(Figure 3) compares energy utilization in the natural gas sweetening process using monoethanolamine solvent with (P2) and without (P1) heat integration. According to this figure, the gas sweetening process with heat integration consumes less energy than when the heat integration is not utilized. The proposed process demonstrates a significant reduction in both hot utility and cold utility by 66.78 percent and 66.77 percent, respectively, when compared to the base process. Consequently, the overall process energy consumption has been effectively diminished by 67 percent. This reduction is computed by comparing the energy consumption of the proposed method (which is the sum of the hot utility, cold utility, and pump work) to that of the basic process. In the proposed process, by introducing side streams of vapor and liquid into the upper and lower sections of the stripping column, the amount of reflux vapor and liquid needed in the column has decreased. This leads to a reduction in the heat duty of the reboiler and condenser. Subsequently, in order to decrease the heat duty of the heater and cooler, the feed entering the heater and cooler is preheated and precooled respectively, using the bottom product of the stripping column and the top product of the absorption column.

Table 3. Equipment Sizing Data

Equipment	Conventional	Heat Integration
T-100 height [ft]	40	40
T-100 diameter [ft]	5.139	5.139
T-101 height [ft]	40	40
T-101 diameter [ft]	873.72	405.6
Heat transfer area of heater [ft^2]	310.52	88.12
Heat transfer area of cooler [ft^2]	4375.36	966.83
Feed rate to pump [m^3/s]	.02766	.02766
Heat transfer area of heat exchanger E-100 [ft^2]	-	2035.5
Heat transfer area of heat exchanger E-102 [ft^2]	-	966.83

Based on the economic analysis results, the proposed process significantly reduces the operating cost due to the decrease in hot and cold utilities. Based on (Table 3), the diameter of the srtripping column in the proposed process is reduced by approximately 50 percent due to the reduced boilup to the stripping column in the proposed process compared to the basic process, thereby decreasing the capital cost as well. Furthermore, the heat transfer area of the cooler in the proposed process was reduced by approximately 78 percrnt because of the pre-cooling of recycled Amine by sweet gas, the distillate product of the absorbtion column. Owing to these reductions in both operating and capital costs, the TAC in the proposed process is lowered by 66.77% in comparison to the basic process even though two heat exchangers were added to the proposed process. (Figure 4) compares the operating cost, capital cost and TAC in the natural gas sweetening process using monoethanolamine solvent with (P2) and without (P1) heat integration.

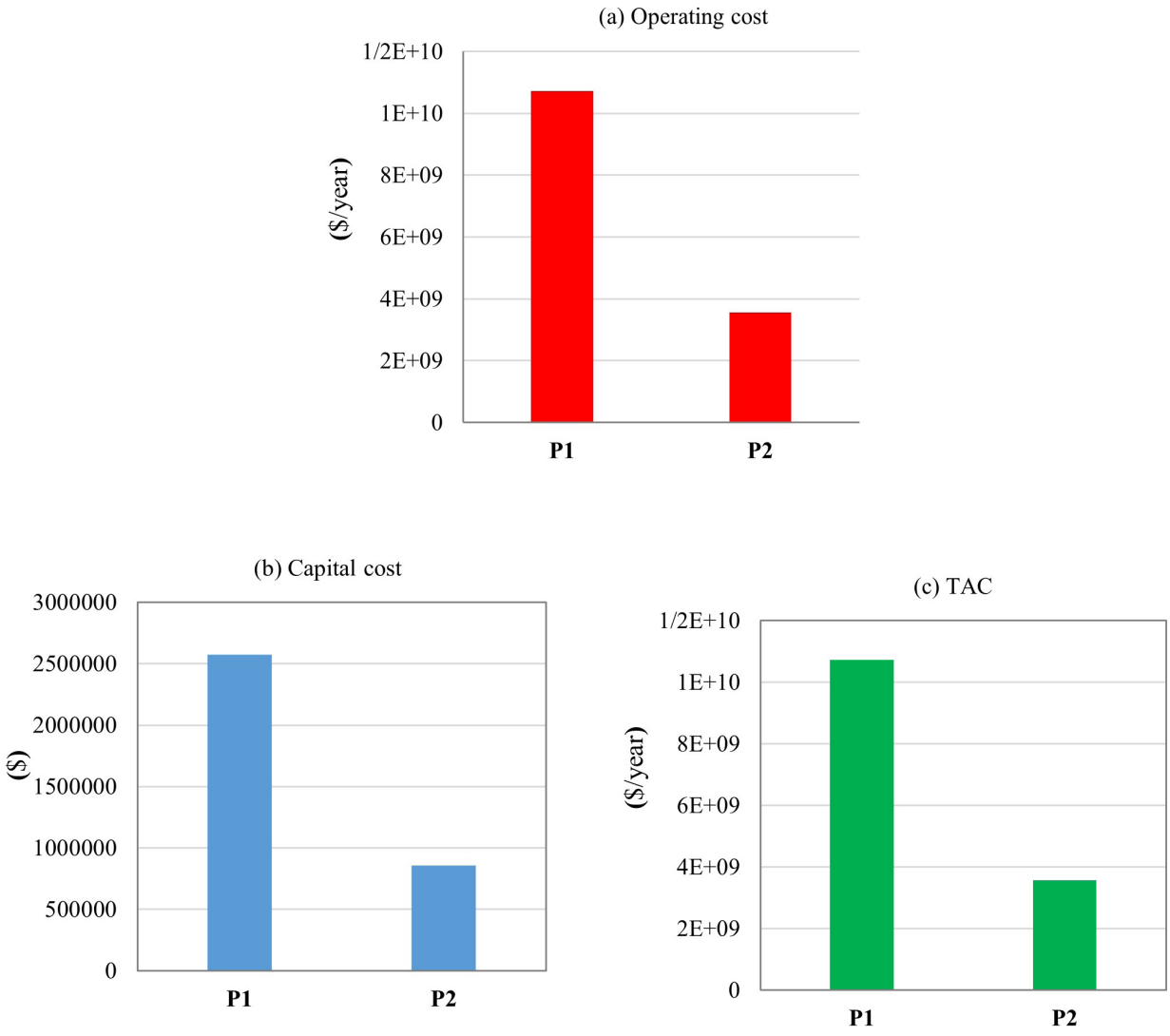

Figure 4. Comparison of Economic Costs (a) Operating Cost, (b) Capital Cost, (c) TAC

4. Conclusions

The natural gas sweetening unit is among the key units in any gas refinery complex. In this unit Hydrogen sulfide (H_2S) and carbon dioxide (CO_2) should be completely removed from the natural gas. A natural gas sweetening unit usually involves an absorption column and a distillation column. monoethanolamine was used in this study to remove H_2S and CO_2. The main problem is high energy consumption in the gas sweetening process so that large part of energy is consumed in the distillation column for amine recovery. Accordingly, energy optimization of this process seems necessary given the global energy crisis in recent years. A novel method was used in this study for heat integration of the natural gas sweetening process. Two side streams from absorption column were used to supply the heat duty of the distillation column. A liquid stream enters the upper part of the distillation column from the lower part of the absorbtion column. A vapor stream leaves the upper part of the absorption column and enters the lower part of the distillation column. The presence of liquid and vapor in the distillation column reduces the heat duties of the reboiler and condenser. The feed entering the distillation column is preheated by its bottom product, reducing the heat duty of the reboiler. The bottom product of the distillation column containing amine is recycled to the absorption column after being precooled by the sweet gas stream, significantly reducing the hot and cold utilities of the process. According to the results, the proposed method reduced the cold and hot utilities of the process by 67%. Significant reduction in energy consumption in the proposed process drastically reduces the amount of vapor and cold water consumed. It significantly reduces the operating costs and thus a significant reduction in TAC, as it concluded after TAC calculations for the two processes. Results indicated that the proposed process could decrease TAC of the base process about 66.77%.

Nomenclature

DEA	diethanolamine
DGA	diglycolamine
DME	dimethoxyethane
MDEA	methyl diethanolamine
MEA	monoethanolamine

Appendix A. Total annual cost calculatione

In this section, the relationships related to cost calculations are presented (Babaie and Esfahany, 2020).

A.1. Cost of Columnn

$$Column\ cost\ [\$] = \frac{M\&S}{280} \times 101.9 \times D_c^{1.066} \times L_c^{0.802} \times (2.18+3.67) \quad (A.1)$$

where D_c [ft] is the diameter of the column and L_c [ft] is the height of column.y, 2020).

A.2. Cost of Tray

$$Tray\ cost\ [\$] = \frac{M\&S}{280} \times 4.7 \times D_c^{1.55} \times L_c \times (1+1.8+1.7) \quad (A.2)$$

Where L_c [ft] is the height of column.

A.3. Cost of Heat Exchanger

$$Heat\ exchanger\ [\$] = \frac{M\&S}{280} \times 101.3 \times A^{0.65} \times (2.29+F_c) \quad (A.3)$$

where A is heat transfer area and F_C is 5.0625 for the reboiler and 3.75 for the condenser.

A.4. Cost of Feed Pump

$$Pump\ cost[\$] = 26700 \times \left(\frac{24 \times F_F \times 3600}{50000}\right)^{0.53} \quad (A.4)$$

where F_F is the total feed rate to the pump [m^3/s].

A.5. Utility Costs

Cooling water = 0.354 ($/GJ)

Low pressure steam (LP) (5 barg, 160 °C) = 13.28 ($/GJ)

High pressure steam (HP) (41 barg, 254 °C) = 17.70 ($/GJ)

References

Al Hatmi, K., Al Mashrafi, A.a., Al Balushi, S.u., Al Battashi, M., 2019. Energy Savings of Amine Sweetening Process Through Rich Solvent Recycle Approach and Low Stripper Operating Pressure, Abu Dhabi International Petroleum Exhibition & Conference. OnePetro.

Babaie, O., Esfahany, M.N., 2020. Optimization and heat integration of hybrid R-HIDiC and pervaporation by combining GA and PSO algorithm in TAME synthesis. Separation and Purification Technology 236, 116288.

Babaie, O., Esfahany, M.N., 2022. Combining game theory and evolutionary algorithms for optimizing hybrid RDWC-pervaporation-vapor permeation process equipped with solar heating system. Journal of Cleaner Production 376, 134235.

Baccanelli, M., Langé, S., Rocco, M.V., Pellegrini, L.A., Colombo, E., 2016. Low temperature techniques for natural gas purification and LNG production: An energy and exergy analysis. Applied energy 180, 546-559.

Chen, S., Fu, Y., Huang, Y., Tao, Z., Zhu, M., 2016. Experimental investigation of CO_2 separation by adsorption methods in natural gas purification. Applied energy 179, 329-337.

Gutierrez, J.P., Ruiz, E.L.A., Erdmann, E., 2017. Energy requirements, GHG emissions and investment costs in natural gas sweetening processes. Journal of Natural Gas Science and Engineering 38, 187-194.

Kazmi, B., Raza, F., Taqvi, S.A.A., Ali, S.I., Suleman, H., 2021. Energy, exergy and economic (3E) evaluation of CO_2 capture from natural gas using pyridinium functionalized ionic liquids: A simulation study. Journal of Natural Gas Science and Engineering 90, 103951.

Kohl, A.L., Nielsen, R., 1997. Gas purification. Elsevier.

Long, N.V.D., Lee, M., 2017. Novel acid gas removal process based on self-heat recuperation technology. International Journal of Greenhouse Gas Control 64, 34-42.

Mohamadi-Baghmolaei, M., Hajizadeh, A., Zahedizadeh, P., Azin, R., Zendehboudi, S., 2021. Evaluation of hybridized performance of amine scrubbing plant based on exergy, energy, environmental, and economic prospects: A gas sweetening plant case study. Energy 214, 118715.

Seo, Y.-j., Park, S., Kang, H., Ahn, Y.-H., Lim, D., Kim, S.-J., Lee, J., Lee, J.Y., Ahn, T., Seo, Y., 2016. Isostructural and cage-specific replacement occurring in sII hydrate with external CO_2/N2 gas and its implications for natural gas production and CO_2 storage. Applied Energy 178, 579-586.

Song, C., Liu, Q., Ji, N., Deng, S., Zhao, J., Kitamura, Y., 2017. Natural gas purification by heat pump assisted MEA absorption process. Applied Energy 204, 353-361.

Tavan, Y., Tavan, A., 2014. Performance of conventional gas sweetening process to remove CO_2 in presence of azeotrope. Journal of CO_2 Utilization 5, 24-32.

JOURNAL OF GAS TECHNOLOGY

Volume 8 /Issue 1 / Summer 2023 / Pages 35-41

Journal Home page: http://jgt.irangi.org

Synthesis and Characterization of Glycidyl Methacrylate-Grafted Ethylene-Propylene Diene Terpolymer Employing Styrene as a Comonomer

Marzieh Alidadi-Shamsabadi[1], Shirin Shokoohi[2*]

1. Chemistry & Chemical Engineering Technical Centre, Academic Centre for Education, Culture and Research (ACECR), Isfahan University of Technology branch, Isfahan, Iran
2. Chemical, Polymeric and Petrochemical Technology Development Research Division, Research Institute of Petroleum Industry, Tehran, Iran

ARTICLE INFO

ORIGINAL RESEARCH ARTICLE

Article History:
Received: 02 July 2023
Revised: 16 August 2023
Accepted: 10 September 2023

Keywords:
Free-radical grafting
Glycidyl Methacrylate
EPDM, Comonomer
Gel contentl

ABSTRACT

Melt free-radical grafting reactions between ethylene-propylene-diene terpolymer (EPDM) and glycidyl methacrylate (GMA) were studied in a batch mixer at 170°C and 60rpm, with and without styrene (St) comonomer. Effect of dicumyl peroxide (DCP) initiator, GMA and styrene concentrations were studied on the grafted EPDM characteristics. Titration results indicated an increase in the graft degree (GD) and gel content (GC) values with increasing DCP concentration. Whereas, introduction of St led to 132% increase in GD and 39% decrease in GC which might be ascribed to its effect on restricting crosslinking side-reaction. FTIR spectrums confirmed that GMA has been successfully grafted onto EPDM.

DOR: 20.1001.1/jgt.2024.2020577.1032

How to cite this article
M. Alidadi-Shamsabadi, S. Shokoohi, Synthesis and Characterization of Glycidyl Methacrylate-Grafted Ethylene-Propylene Diene Terpolymer Employing Styrene as a Comonomer. Journal of Gas Technology. 2023; 8(1): 35-41. (https://jgt.irangi.org/article_718890.html)

* Corresponding author.
E-mail address: shokoohish@ripi.ir, (S. Shokoohi).

Available online 20 September 2023

1. Introduction

The inert nature of most polymers is the key characteristic allowing for their considerable use in variety of applications, but at the same time a disadvantage for applications in which surface wettability or interaction with polar components is required (Oxley, Gaffney, 2022, Passaglia, Coiai, 2009, Sun, Liu, 2020). In order to obviate this problem, several studies have been conducted on the functionalization of polymers (e.g. polyolefins, polyesters, etc.) through free-radical grafting of functional monomers onto the polymer backbone.

Free-radical grafting of functional monomers onto polyolefins is always accompanied with side reactions depending on the nature of macro-radicals and the polyolefin. Chain branching/crosslinking and chain scission are the most common side reactions detected for polyethylene and polypropylene, respectively (Marsilla and Verbeek, 2015). Introducing a second monomer such as styrene (Ma, Cai, 2014), divinyl benzene (DVB) (Doudin, Ahmad, 2009) and trimethylolpropanetriacrylate (Tris) (Al-Malaika and Kong, 2001) to the grafting reactions as "comonomer" or "co-agent" is suggested to control undesirable side reactions. Comonomer are shown to decrease the gel content dramatically where a little effect on the grafting degree have been reported (Li, Zhang, 2003). However, there are no reports on the compatibilization of EPDM using styrene as a comonomer or co-agent. According to the mentioned gap in the grafting process of EPDM, styrene-assissted free-radical grafting reactions at different dicumylperoxide initiator and GMA concentrations were investigated in the present study. Grafting degree and gel content of EPDM rubber samples functionalized at the absence and presence of styrene comonomer were analyzed through FTIR and titration techniques.

2. Experimental

2.1. Materials

Materials used in this research were ethylene propylene diene monomer (EPDM), KEP 270 supplied by KumhoPolychem (Korea)with mooney viscosity ML (1 + 4) 125 °C: 71M, ethylene content: 57%, termonomer content: 4.5 ENB%, density: 0.86 g/cm^3; glycidyl methacrylate monomer (GMA, 97%, Aldrich Chemical Co., Japan); dicumyl peroxide (DCP, 98%, Merck Millipore, Germany) and styrene monomer (st., 99%, Merck Millipore, Germany). Xylene, acetone, ethanol, trichloroacetic acid (TCA), phenolphthalein and potassium hydroxide used for titration and purification were all of analytical grade obtained from Merck Millipore.

2.2. Preparation

Melt grafting reactions were conducted using an internal mixer (Brabender W50, Duisburg, Germany) preheated to 170 °C. Regarding the volatility of GMA at the processing temperature, twenty minutes prior to the mixing, GMA, DCP initiator and styrene chain-transfer agent (for styrene-assisted batches) were physically poured on EPDM in a closed container. Impregnated EPDM was then melt mixed for 8 minutes at 60 rpm. This process can be seen in (Figure 1). All EPDM-g-GMA samples were prepared according to (Table 1) (Jazani, Rastin, 2017).

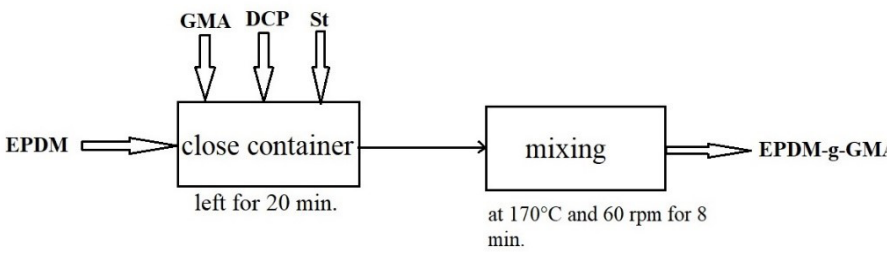

Figure 1. Melt Free-Radical Grafting Process

Table1. Melt Free-Radical Grafting Components: Concentrations and Nomencalture

Sample Code	DCP, phr	GMA, phr	St, phr
E-St-1	0.5	3	2.25
E-St-2	0.5	5	3.75
E-St-3	0.5	7	5.25
Blank1	0	5	0
E1	0.5	5	0
E2	0.3	5	0
Blank2	0	3	0
E3	0.3	3	0
E4	0.15	3	0

2.3. Characterization

Gel content and graft degree measurements- A few grams of each EPDM-g-GMA sample was put in 100 ml boiling xylene for one hour. The remaining solid filtrate was dried in vacuum oven at 80 °C for 24 hours. Gel content was then calculated according to the following Equation:

$$GC = \frac{w_1}{w_0} \times 100 \quad (1)$$

Where w_0 and w_1 are sample weights before and after xylene solution, respectively.

Graft degree was calculated according to Eq. (2) (Alidadi-Shamsabadi, Arefazar, 2020):

$$GD = \frac{142.15 \times (C_0V_0 - C_2V_2)}{W} \times 100 \quad (2)$$

Where C_0 and C_2 are TCA and KOH standard solution concentration, respectively. V_0 and V_2 are TCA standard solution volume and KOH standard solution volume used through titration, respectively. Windicates the initial sample weight. Fourier transform infrared (FTIR) spectroscope (Bomem-102, Canada) was used to track the expected reactions. Samples were purified with boiling xylene and acetone/ethanol anti-solvent before acetone rinsing to prepare the test sample:

3. Results and Discussion

3.1. Gel Contact and Degree of Grafting

(Figure 2) compares the variations observed in gel content and GMA graft degree with increasing DCP amount at fixed GMA contents, for those samples prepared with no styrene. At both GMA contents studied here (i.e. 3 and 5 phr); a similarly increasing trend is observed for graft degree values versus DCP content. This is attributed to the accelerated formation of free-radicals and consequently macro-radicals along the polymer chain at the presence of DCP. In fact, the DCP initiator undergoes a homolytic decomposition upon thermomechanical heating to yield a pair of primary free radicals which can abstract a tertiary hydrogen from the EPDM chain to form a macromolecular radical (Brito, Xin, 2014).

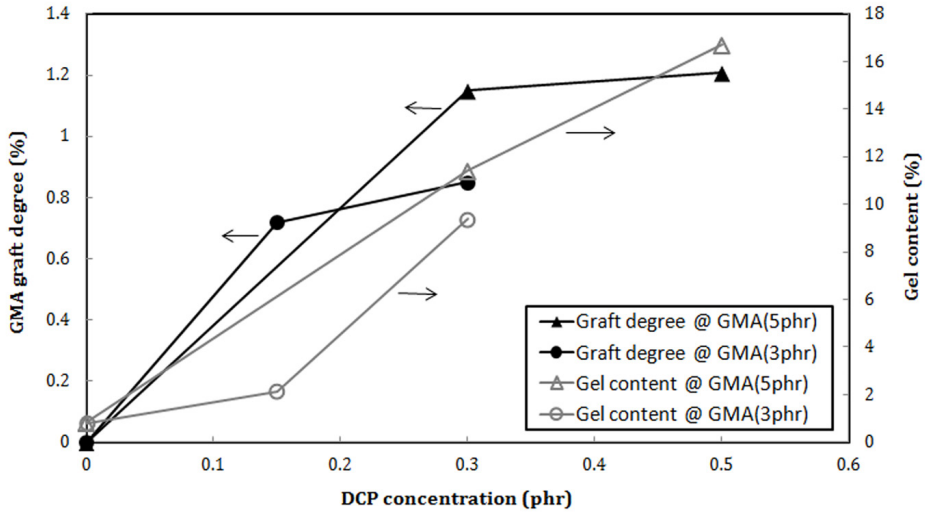

Figure 2. GMA Grafted EPDM, Graft Degree and Gel Content Versus DCP Concentration at Different GMA Concentrations

Gel content has also increased with DCP content at the same time with the graft degree but the trend is somehow different. At GMA content of 5 phr, the increasing rate is almost uniform along all DCP contents studied here, since crosslinking competing reactions would be more contingent at the presence of higher concentrations of macro-radicals. This would produce more gel-like structures in the sample bulk. At GMA contents of 5 phr, the increasing rate was observed to be unaffected by DCP concentration which might be due to the homo-polymerization of GMA molecules beside the crosslinking reactions. In such circumstances, a portion of the free-radicals present in the reaction media are involved in the GMA homo-polymerization. This would suppress the expected crosslinking reactions. Limited solubility of monomer in the polymer, yielding high local concentration, has also known to be responsible for oligo(GMA) grafts (Gross, Schneider, 2018).

Comparing the values presented in (Figure 2) and (Table 2) for E-St-1, E-St-2 and E-St-3 with those of E1, E2, E3, E4, Blank1 and Blank2 shows that the graft degree and gel content of the samples prepared at the presence of styrene chain-transfer agent are respectively greater and smaller than the samples prepared without styrene.

Table2. Graft Degree and Gel Content of EPDM Samples Grafted at the Presence of Styrene (DCP=0.5 phr)

Sample Code	Graft Degree,%	Graft Efficiency,%	Gel Content,%
E-St-1	1.93	64.3	8.51
E-St-2	2.81	56.2	10.12
E-St-3	3.04	43.4	10.68

It should be noted that the direct attack of the macroradicals to GMA is significantly hindered by the steric effect of polymer chains where in the presence of styrene comonomer; the EPDM macroradicals preferably attack styrene due to its less steric effect. Produced styryl radicals, then, are copolymerized with GMA monomers easily. On the other hands, styrene could progress a reaction with EPDM macro-radicals much faster than GMA and this would prevent the macro-

radicals to be involved in the crosslinking competing pathways. The resulting styryl macroradicals are also stabilized by resonance of styrene. This procedure would cause an increase in the graft degree (Bansod, Kapgate, 2018).

According to (Table 2), a moderate increase can be seen in the gel content by simultaneously increasing equimolar amounts of GMA and St, as well the graft efficiency has decreased. While GMA (positive on GD, negative on GC) and St (positive on GD and GC) effects have been individually investigated, the equimolar amount of GMA introduced to the reaction seems to negatively affect the reaction. Accordingly, to achieve acceptable gel contents and graft efficiencies, St/GMA molar ratios greater than 1 seem to be more sensible. Considering that styrene, besides the direct reaction with macroradicals, could activate the graft monomer (i.e. GMA) by forming a charge-transfer complex;(Brito, Xin, 2014) introducing St/GMA molar ratios smaller than 1 might restrict the styrene comonomer roles. Flat(Hu, Flat, 2012) correspondingly showed that grafting yield does not always increase with styrene content but it goes through a maximum when St/GMA molar ratio is between 1 and 2.

3.2. FTIR Spectroscopy

(Figure 3a) compares the FTIR spectroscopy results of pure EPDM and the EPDM samples grafted by GMA in the absence of styrene comonomer. As expected, the main characteristic peak confirming the formation of C = O carbonyl groups during the grafting reaction, has appeared at 1730 cm-1 for samples E1, E2, E3 and E4. Although Bray (Bray, Damiris, 1998) believed that formation of oligo(maleic anhydride) grafts would shift the characteristic peak of simple alkyl succinates; no evidence reliable enough to claim the formation of graft length was detected here. The epoxy group, responsible for the compatibilizing features of GMA-grafted polymers, was detected as a shoulder at 990 cm-1.

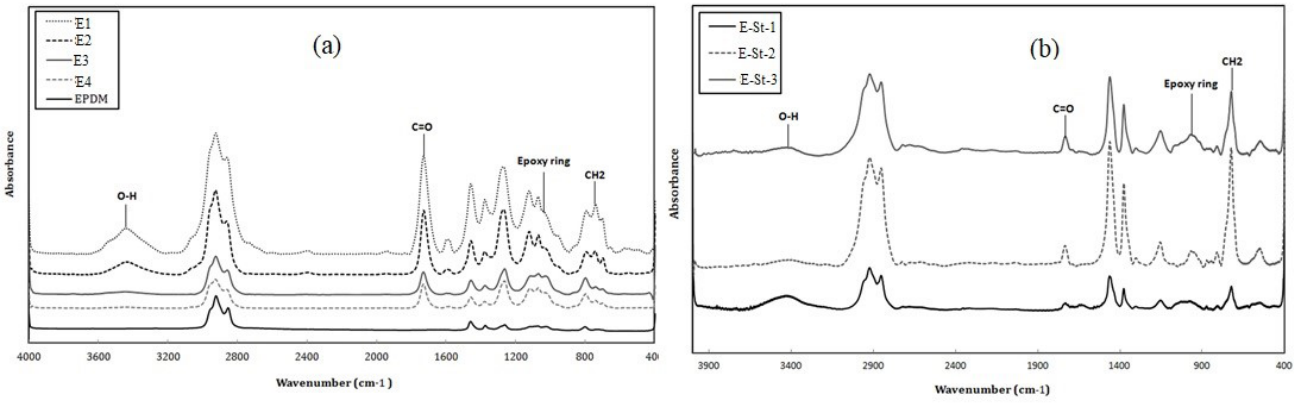

Figure 3. FTIR results of pure EPDM and the EPDM-g-GMA samples in the (a) absence and (b) presence of styrene

FTIR spectroscopy results of EPDM-g-GMA samples prepared in the presence of styrene comonomer are illustrated in (Figure 3b). Peaks appeared at 721, 972, 1734 and 3433 respectively correspond to stretching CH_2, epoxide, carbonyl and hydroxyl functions confirming the functionalization of EPDM chains by GMA.

4. Conclusion

Glycidylmethacrylate was grafted onto ethylene-propylene-dieneterpolymer through melt free-radical grafting process in the absence and presence of styrene chain-transfer agent. Graft degree and gel content results obtained by titration indicated that styrene improves the

graft degree by preventing the unfavorable crosslinking reactions. The decrease in gel content values confirms this observation. Comparing the results published on the application of trimethylolpropanetriacrylate shows that styrene shows a better performance decreasing the gel content besides its positive effect on the graft degree. In the absence of styrene, increasing the concentration of DCP can improve the graft degree as well as the gel content. Analyzing the graft degree and gel content results showed that sample E4 (DCP = 0.15 phr, GMA = 3 phr) with grafting degree of 0.72 wt% and gel content of 2.12 wt% could be selected as the best sample to use as a compatibilizer in polymer blends. FTIR results confirmed the conclusions based on titration technique.

List of Abbreviation

DCP	Dicumyl peroxide
EPDM	Ethylene-propylene-diene terpolymer
EPDM-g-GMA	Glycidyl methacrylate grafted Ethylene-propylene-diene terpolymer
FTIR	Fourier transform infrared
GC	Gel content
GD	Graft degree
GMA	Glycidyl methacrylate

References

Al-Malaika, S. and W. Kong, 2001. Reactive processing of polymers: Melt grafting of glycidyl methacrylate on ethylene propylene copolymer in the presence of a coagent. J. Appl. Polym. Sci. 79, 1401-1415.

Alidadi-Shamsabadi, M., A. Arefazar, and S. Shokoohi, 2020. IMPROVEMENTS IN THE SYNTHESIS AND CHARACTERIZATION OF GLYCIDYL METHACRYLATE-GRAFTED EPDM THROUGH MELT FREE-RADICAL PROCESS. Rubber chem. technol. 93, 222-234.

Bansod, N.D., et al., 2018. FUNCTIONALIZATION OF EPDM RUBBER TOWARD BETTER SILICA DISPERSION AND REINFORCEMENT. Rubber Chem. Technol. 92, 219-236.

Bray, T., et al., 1998. Developments in the synthesis of maleated polyolefins by reactive extrusion. Macromol. Symp. 129, 109-118.

Brito, G.F., et al., 2014. Enhanced melt free radical grafting efficiency of polyethylene using a novel redox initiation method. RSC Advances 4, 26425-26433.

Doudin, K., A. Ahmad, and S. Al-Malaika, 2009. Reactive processing of polymers: Structural characterisation of products by 1H and 13C NMR spectroscopy for glycidyl methacrylate grafting onto EPR in the absence and presence of a reactive comonomer. Polym. Degrad. Stab. 94, 1599-1614.

Gross, I.P., et al., 2018. Polylactic acid, maleic anhydride and dicumyl peroxide: NMR study of the free-radical melt reaction product. Polym. Degrad. Stab. 155, 1-8.

Hu, G.-H., Flat J.J., and Lambla M., 2012. Free-radical grafting of monomers onto polymers by reactive extrusion: principles and applications, in Reactive modifiers for polymers, Springer Science & Business Media, London.

Jazani, O.M., et al., 2017. An investigation on the role of GMA grafting degree on the efficiency of PET/PP-g-GMA reactive blending: morphology and mechanical properties. Polym. Bull. 74, 4483-4497.

Li, C., Y. Zhang, and Y. Zhang, 2003. Melt grafting of maleic anhydride onto low-density polyethylene/polypropylene blends. Polym. Test. 22, 191-195.

Ma, P., et al., 2014. Styrene-assisted melt free-radical grafting of maleic anhydride onto poly (β-hydroxybutyrate). Polym. Degrad.

Stab. 100, 93-100.

Marsilla, K.K. and C. Verbeek, 2015. Modification of poly (lactic acid) using itaconic anhydride by reactive extrusion. Eur. Polym. J. 67, 213-223.

Oxley, A., et al., 2022. Graft modification of polybenzimidazole membranes for organic solvent ultrafiltration with scale up to spiral wound modules. J. Membr. Sci. 647, 120199.

Passaglia, E., S. Coiai, and S. Augier, 2009. Control of macromolecular architecture during the reactive functionalization in the melt of olefin polymers. Prog. Polym. Sci. 34, 911-947.

Sun, W., et al., 2020. Chemical surface modification of polymeric biomaterials for biomedical applications. Macromol. Rapid Commun. 41, 1900430.

شبیه سازی عددی در یک رژیم دینامیکی جریان گاز طبیعی در شبکه خط لوله

- راباح هاوئی*

گروه انرژی حرارتی، دانشگاه علوم و فناوری هواری بومدین، الجزیره، الجزایر

(ایمیل نویسنده مسئول: haoui_rabah@yahoo.fr)

چکیـــــــده

هدف از این مقاله ارائه نظری برای آشکارسازی فشار و جریان عرضه در حالت مصرف در رژیم دینامیک می باشد. مدل ریاضی سیستمی از معادلات دیفرانسیل غیرخطی است که با یک جریان تراکم پذیر با اصطلاح افت فشار سروکار دارد، دما ثابت و برابر با محیط در نظر گرفته می شود. شرایط مرزی داده شده و راه حل اولیه نامشخص است، پس از حل گذرا، حالت دینامیکی دوره ای به صورت پایدار برقرار می شود. روش گسسته‌سازی مورد استفاده، تفاوت‌های ظریف با مش ساختار یافته است. روش تفکیک نیمه ضمنی با یک مرحله زمانی است که به شدت به تعداد CFL بستگی دارد که همگرایی را تضمین می کند. روش انتخاب شده در طول زمان پایدار است. نتایج اصلی به دست آمده اعتبار روش مورد استفاده برای حل یک مسئله دینامیکی، دقت محاسبات و پدیده فیزیکی است که به وضوح از توزیع فشارها و نرخ جریان به عنوان تابعی از زمان و موقعیت قابل مشاهده است.

واژگان کلیدی: مصرف گاز طبیعی، شبکه گاز طبیعی، جریان ناپایدار، جریان تراکم پذیر، رژیم دینامیکی، روش تفاضل محدود

بررسی جذب متان در چارچوب‌های فلزی-آلی MIL با استفاده از شبیه‌سازی دینامیک مولکولی

- سامان بنی جمالی[1]، هدایت عزیزپور[2*]، پریسا خدیوپارسی[2]

۱. دانشجوی کارشناسی ارشد مهندسی شیمی، دانشکده مهندسی شیمی، دانشکدگان فنی، دانشگاه تهران ، تهران، ایران

۲. استادیار، دانشکده مهندسی شیمی، دانشکدگان فنی، دانشگاه تهران ، تهران، ایران

(ایمیل نویسنده مسئول: h.azizpour@ut.ac.ir)

چکیـــــــده

در این مطالعه، خواص جذب سه چارچوب فلز-آلی MIL-101 (Cr)، MIL-100 (Fe) و MIL-100 (Al) برای ذخیره‌سازی متان با فشار بالا در گاز طبیعی جذب شده بررسی شد. با استفاده از نرم‌افزار Materials Studio و شبیه‌سازی مونت‌کارلو، شبیه‌سازی دینامیک مولکولی تحت‌فشار ثابت ۳۵ اتمسفر و دمای ۳۰۰ کلوین انجام شد. میزان جذب به ترتیب ۰/۰۰۸، ۰/۰۸۹ و ۰/۰۳۵ گرم متان در هر گرم جاذب برای MIL-101 (Cr)، MIL-100 (Fe) و MIL-100 (Al) گزارش شد. برای تأیید یافته‌ها، ظرفیت جذب محاسبه‌شده MIL-101 (Cr) با داده‌های تجربی مقایسه شد که تطابق نزدیک با مقدار گزارش شده ۰/۰۳۶ گرم متان در هر گرم جاذب نتیجه شد. شبیه‌سازی‌ها همچنین بینش‌هایی را در مورد الگوهای جذب آشکار کردند و نشان دادند که مولکول‌های متان به‌طور انتخابی با مناطق مختلف چارچوب‌ها بر اساس جهت‌گیری‌شان برهمکنش دارند. این مطالعه نشان می‌دهد که MOFها به‌عنوان جاذب‌های مناسب برای ذخیره‌سازی گاز طبیعی در فناوری‌های ANG نوید دارند. در میان سه MOF مورد مطالعه، MIL-100 (Al) به‌عنوان کارآمدترین گزینه ظاهر شد که با توجه به ملاحظات اقتصادی و تولیدی، پتانسیل را برای پیاده‌سازی در مقیاس صنعتی آینده ارائه می‌دهد.

واژگان کلیدی: چارچوب فلز-آلی (MOF)، جذب متان، فناوری گاز طبیعی جذب شده (ANG)، شبیه‌سازی دینامیک مولکولی، شبیه‌سازی مونت‌کارلو

ارائه یک روش جدید در انتگراسیون حرارتی فرآیند شیرین‌سازی گاز طبیعی

- احسان فاتحی، پریسا سادات فاطمی، محمدجواد زرکش، مهشید مرادی، شهاب طالقانی، مهسا مجیدی*

گروه مهندسی شیمی، موسسه آموزش عالی آزاد پژوهش، تهران، ایران

(ایمیل نویسنده مسئول: mahsamajidi94@gmail.com)

چکیـــــــده

واحد شیرین‌سازی گاز طبیعی عموماً دارای یک برج جذب و یک برج تقطیر است به‌طوری‌که از برج جذب برای حذف کامل گازهای H_2S و CO_2 از گاز طبیعی و از برج تقطیر برای بازیابی حلال استفاده می‌شود. مشکلی که وجود دارد این است که میزان انرژی مصرفی فرآیند شیرین‌سازی گاز به‌ویژه برج تقطیر آن بسیار بالا است. بنابراین بهینه‌سازی انرژی این فرایند الزامی است. در این مقاله از یک روش جدید برای انتگراسیون حرارتی فرآیند شیرین‌سازی گاز طبیعی استفاده شده است. بدین منظور دو جریان مایع و بخار از برج جذب خارج‌شده و به ترتیب وارد بخش بالای برج و بخش پایین برج می‌شوند. همچنین خوراک ورودی به برج تقطیر به کمک محصول پایین برج پیش‌گرم می‌شود. حضور دو جریان مایع و بخار باعث کاهش مصرف یوتیلیتی سرد و گرم در برج تقطیر می‌شود و پیش‌گرم کردن خوراک نیز بار حرارتی ریبویلر را کاهش می‌دهد. سپس حلال برگشتی به کمک گاز شیرین پیش سرد می‌شود. نتایج نشان می‌دهد روش پیشنهادی مقدار انرژی مصرفی فرآیند را به میزان ۶۷ درصد کاهش می‌دهد. علاوه بر این، فرایند پیشنهادی می‌تواند هزینه کل سالیانه (TAC) را نسبت به فرایند پایه به مقدار ۶۶,۷ درصد کاهش دهد. این کاهش هزینه کل سالیانه (TAC) ناشی از کاهش هزینه عملیاتی و هزینه سرمایه‌گذاری به ترتیب به میزان ۶۶,۷۷ و ۶۶,۶۴ درصد است.

واژگان کلیدی: شیرین‌سازی گاز طبیعی، مونو اتانول آمین، انتگراسیون حرارتی، کاهش مصرف یوتیلیتی

سنتز و مشخصه‌یابی اتیلن پروپیلن‌دی ان مونومر پیوند خورده با گلایسیدیل‌متاکریلات از طریق کومونومر استایرن

- مرضیه علیدادی شمس آبادی[۱]، شیرین شکوهی[۲*]

۱. مرکز فنی شیمی و مهندسی شیمی، جهاد دانشگاهی واحد صنعتی اصفهان، اصفهان، ایران

۲. پژوهشکده توسعه فناوری‌های شیمیایی، پلیمری و پتروشیمیایی، پژوهشگاه صنعت نفت، تهران، ایران

(ایمیل نویسنده مسئول: shokoohish@ripi.ir)

چکیـــــــده

واکنش پیوند رادیکال آزاد مذاب بین اتیلن-پروپیلن-دی ان مونومر (EPDM) و گلیسیدیل متااکریلیت (GMA) در حضور و غیاب کومونومر استایرن (St) در مخلوط‌کن داخلی (۱۷۰ سیلسیوس، ۶۰ دور بر دقیقه) بررسی شد. اثر غلظت آغازگر دی کیومیل پراکساید (DCP)، GMA و St بر پیوند بین EPDM و GMA مطالعه شد. نتایج تیتراسیون افزایش مقادیر درجه پیوند (GD) و میزان ژل (GC) را با افزایش غلظت DCP نشان داد. در حالی که کاربرد St، با جلوگیری از ورود ماکرورادیکال‌ها به واکنش جانبی ژل شدن، منجر به افزایش ۱۳۹درصد برای GD و کاهش ۳۹درصد برای GC شد. نتایج FTIR پیوند GMA بر روی زنجیره‌های EPDM را تائید کرد.

واژگان کلیدی: پیوند رادیکال آزاد، گلایسیدیل متاکریلات، اتیلن-پروپیلن-دی ان مونومر، کومونومر، میزان ژل

Iran Gas Institute

Journal of Gas Technology

VOLUME 8 • ISSUE 1 • SUMMER 2023

EISSN: 2588-5596

Contents

1 **Numerical Simulation in a Dynamic Regime of Natural Gas Flow in the Pipeline Networ**

Rabah Haoui

2 **Probing Methane Adsorption in MIL Metal-Organic Frameworks using Molecular Dynamics Simulations**

Saman Banijamali, Hedayat Azizpour, Parissa Khadiv-parsi

3 **A Novel Method for Heat Integration of Natural Gas Sweetening Process**

Ehsan Fatehi, Parisa Sadat Fatemi, Mohammad Javad Zarkesh, Mahshid Moradi, Shahab Taleghani, Mahsa Majidi

4 **Synthesis and Characterization of Glycidyl Methacrylate-Grafted Ethylene-Propylene Diene Terpolymer Employing Styrene as a Comonomer**

Marzieh Alidadi-Shamsabadi, Shirin Shokoohi